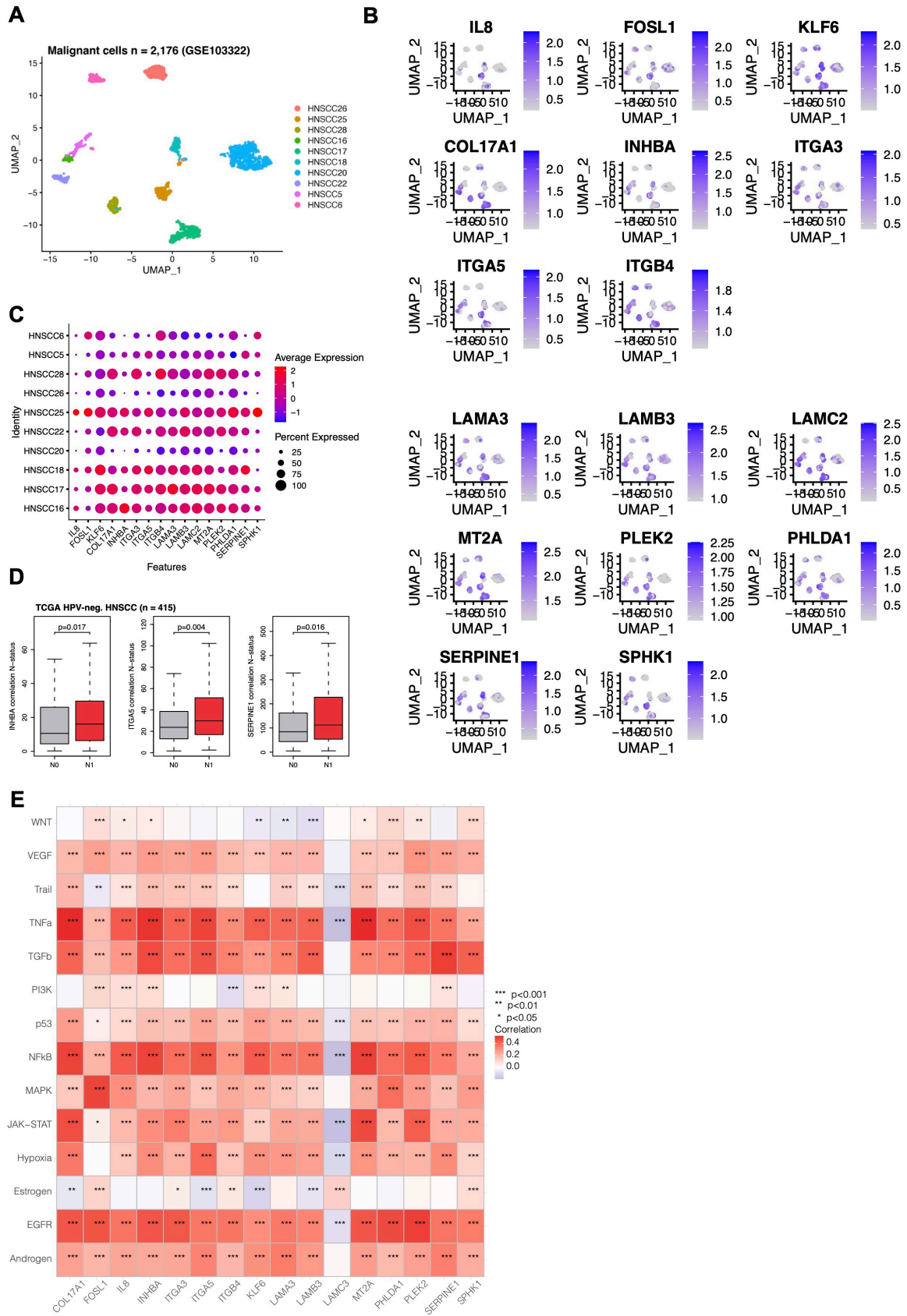


## Supplementary Figures

### EGFR-mediated Local Invasiveness and Response to Cetuximab in Head and Neck Cancer

*Jiefu Zhou<sup>1,2,3,4,\*</sup>, Min He<sup>1,\*</sup>, Qiong Zhao<sup>1,\*</sup>, Enxian Shi<sup>1,\*</sup>, Hairong Wang<sup>1</sup>, Vaidehi Ponkshe<sup>1</sup>, Jiahang Song<sup>1</sup>, Zhengquan Wu<sup>1</sup>, Dongmei Ji<sup>5</sup>, Gisela Kranz<sup>1</sup>, Anna Tscherne<sup>1</sup>, Sabina Schwenk-Zieger<sup>1</sup>, Nilofer Abdul Razak<sup>1</sup>, Julia Hess<sup>6,7</sup>, Claus Belka<sup>7,8</sup>, Horst Zitzelsberger<sup>6</sup>, Iordanis Ourailidis<sup>9</sup>, Fabian Stögbauer<sup>10</sup>, Melanie Boxberg<sup>10</sup>, Jan Budczies<sup>9</sup>, Christoph A. Reichel<sup>1</sup>, Martin Canis<sup>1,8</sup>, Philipp Baumeister<sup>1,8</sup>, Hongxia Wang<sup>5</sup>, Kristian Unger<sup>7</sup>, Andreas Mock<sup>8</sup>, and Olivier Gires<sup>1</sup>*

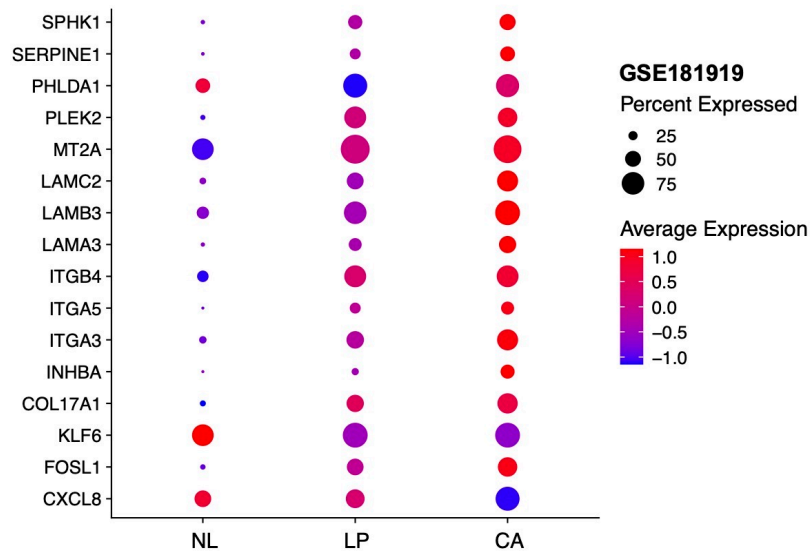


**Suppl. Figure 1: Expression of fDEGs in GSE103322**

(A) UMAP of malignant cells (n = 2,176) from n = 10 OSCC patients (GSE103322). (B) UMAP representation of n = 16 fDEGs in malignant cells of GSE103322. (C) Dot plot of fDEG expression in n = 10 OSCC patients (GSE103322) showing average expression and percent of positive single cells. (D) Bloxplot-whiskers graphs of the expression of *INHBA*, *ITGA5*, and *SERPINE1* in nodal metastases-

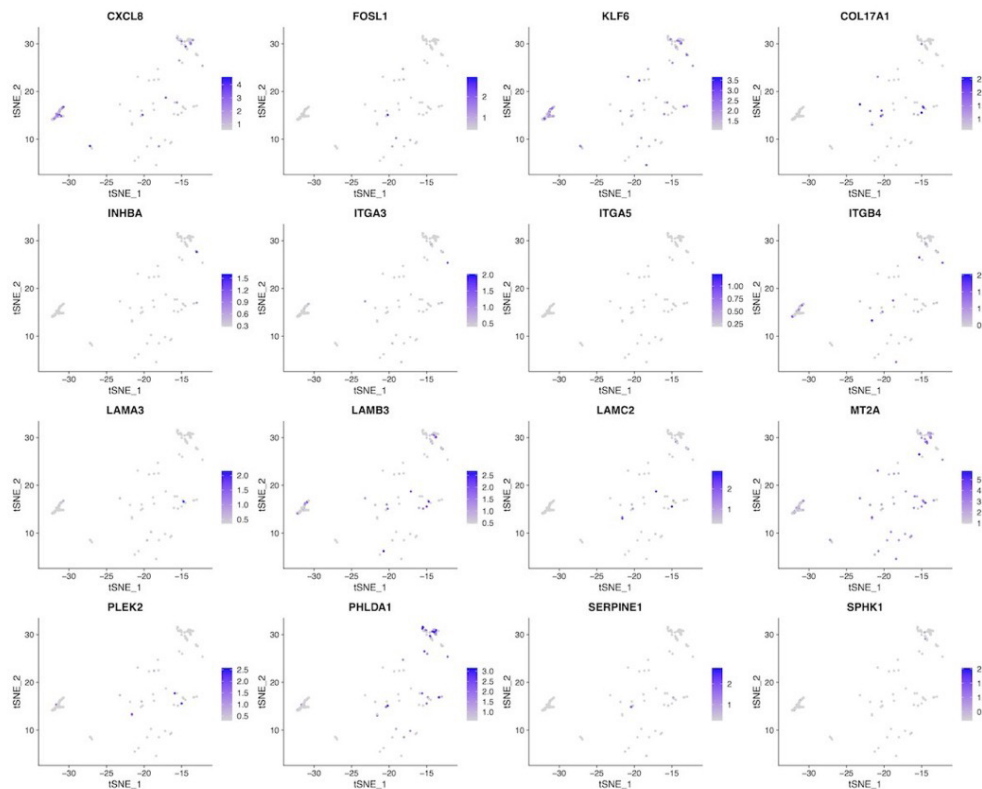
negative (N0) and -positive (N1) patients of the HPV-neg. HNSCC-TCGA cohort. **(E)** Heatmap of correlations of  $n = 16$  fDEGs with signaling pathways within PROGENy with correlation and p-values.

**A**

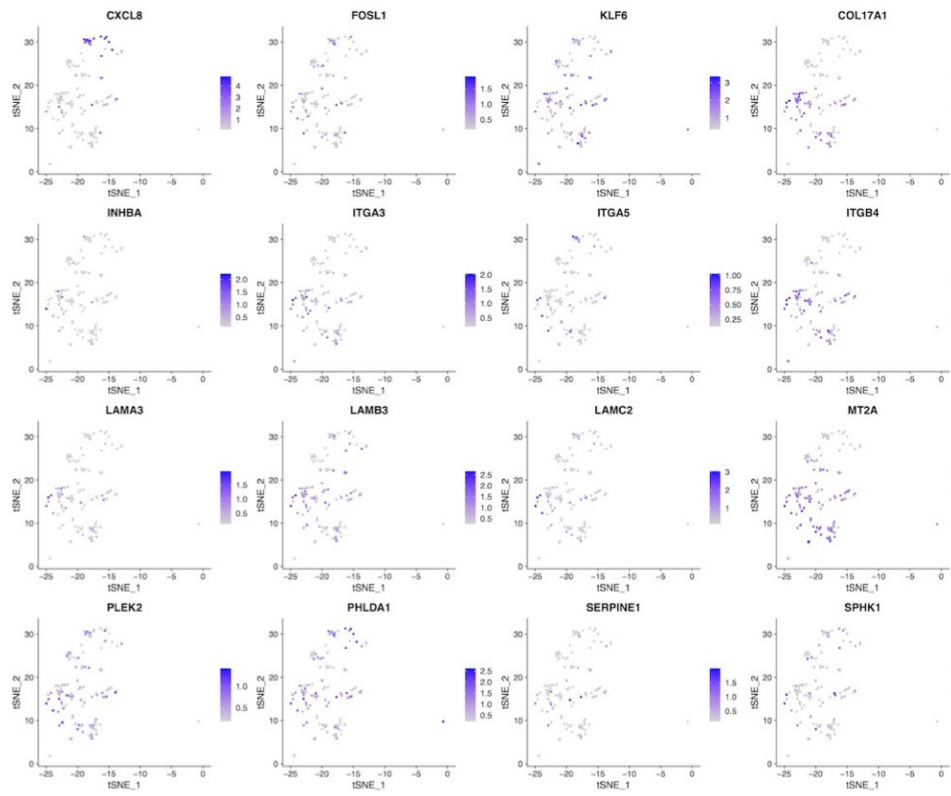


**B**

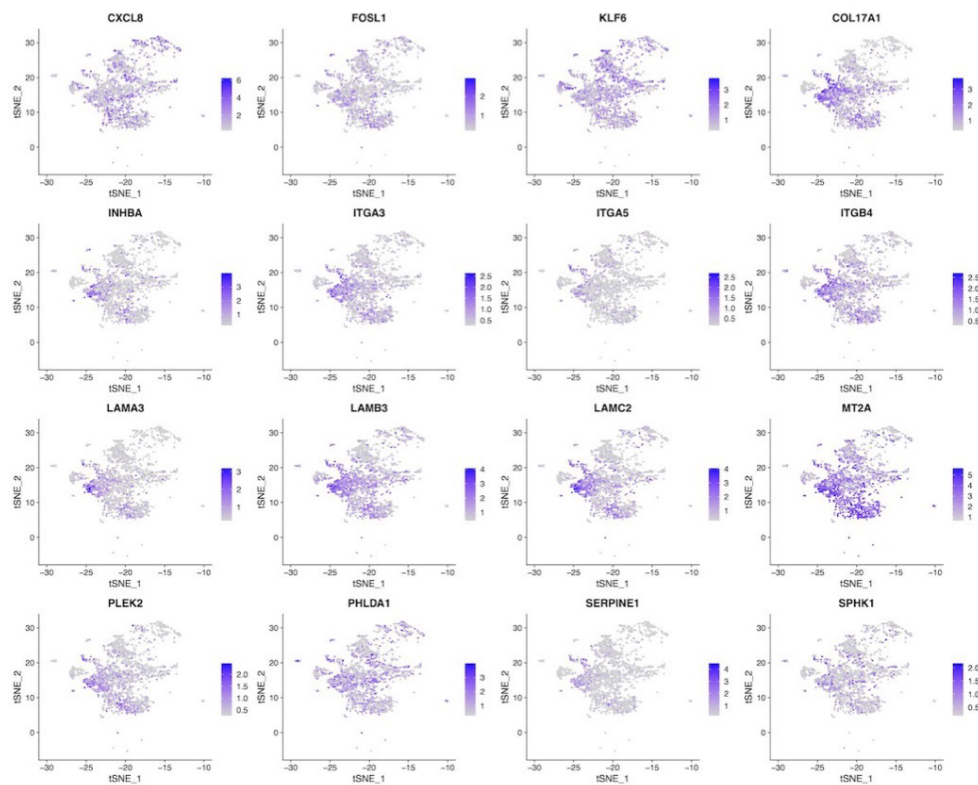
**Normal**



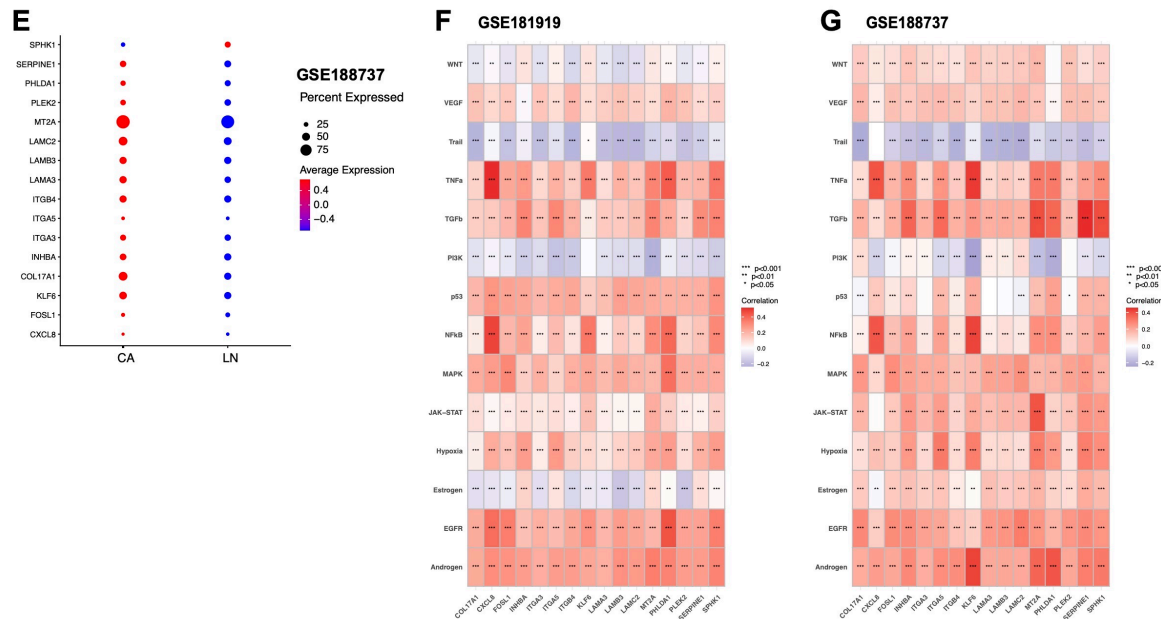
## C Leucoplakia



## D Carcinoma



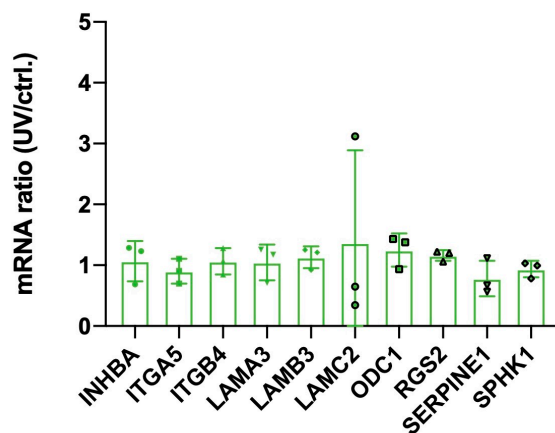




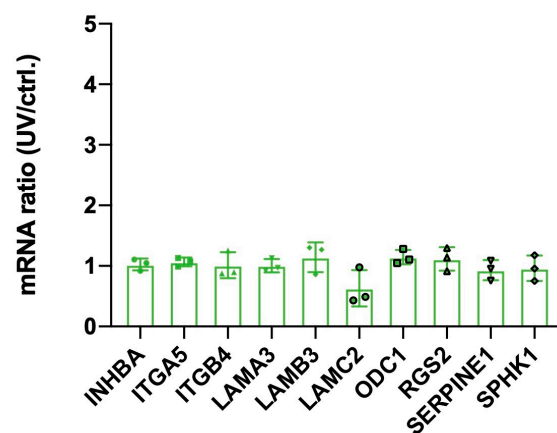
**Suppl. Figure 2: Expression of fDEGs in GSE181919**

(A) Dot plot of fDEGs expression in normal epithelial cells (NL), leucoplakia (LP), and primary HNSCC (CA) (GSE181919) showing average expression and percent of positive single cells. (B-D) UMAP representation of  $n = 16$  fDEGs in normal epithelial cells (B), leucoplakia (C), and malignant cells (D). (E) Dot plot of fDEG expression in primary HNSCC (CA) and nodal metastases (LN) (GSE188737) showing average expression and percent of positive single cells. (F, G) Heatmap of correlations of  $n = 16$  fDEGs with signaling pathways within PROGENy with correlation and p-values from GSE181919 (F) and GSE188737 (G).

### FaDu

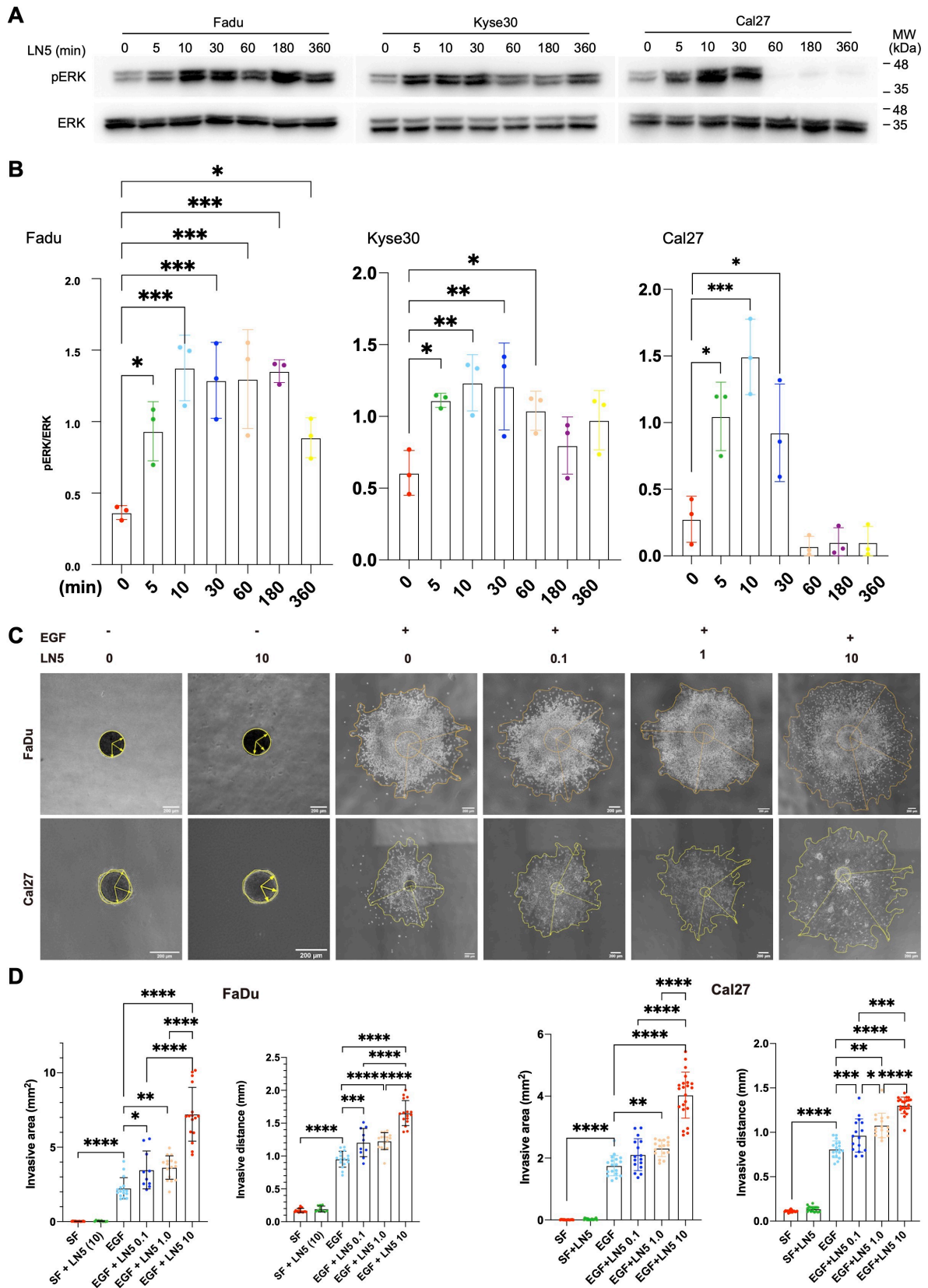


### Ky30



**Suppl. Figure 3: Effects of UV-irradiation on gene expression of selected functional differentially expressed genes (fDEGs)**

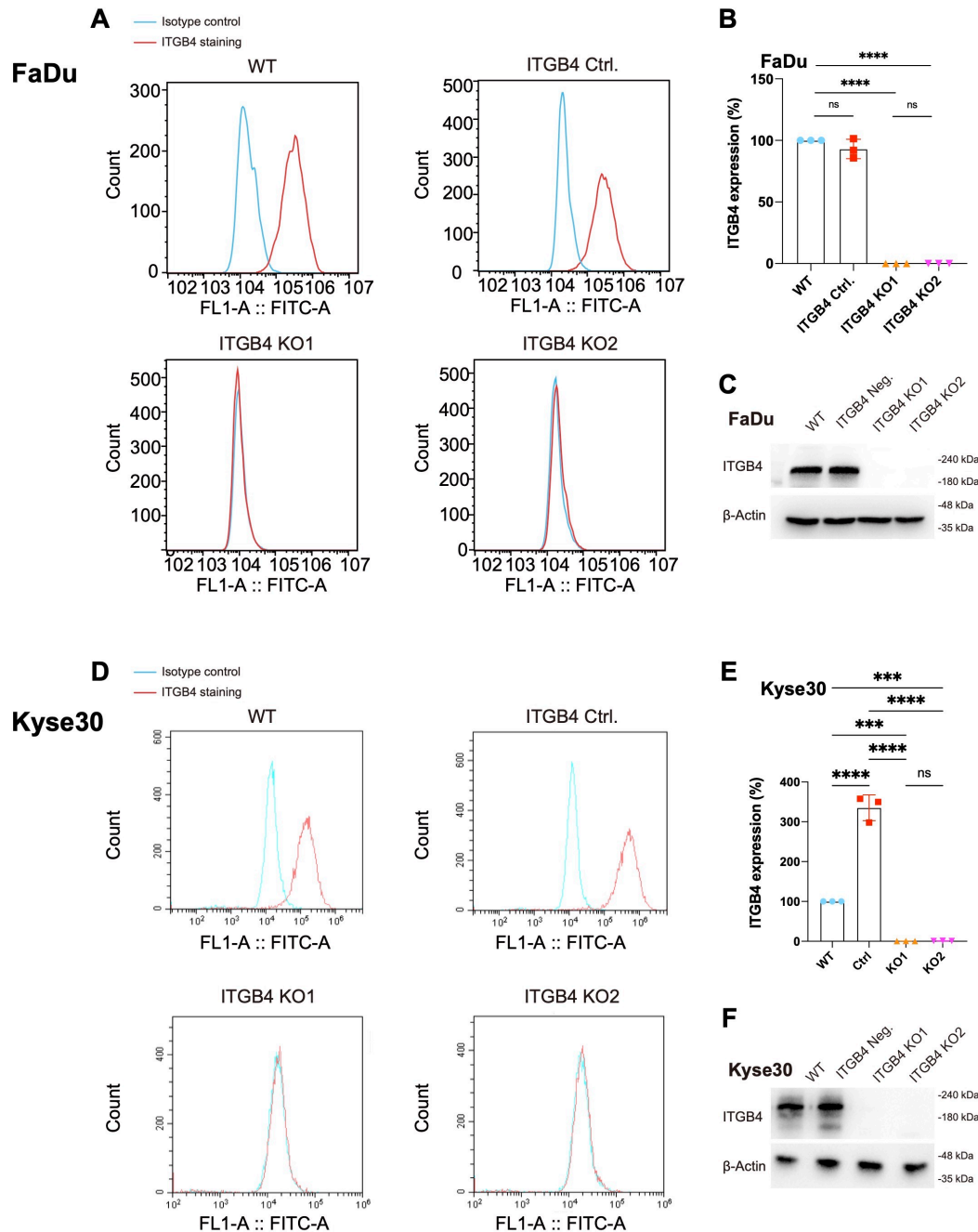
FaDu-Dendra2 and Kyse30-Dendra2 cells were grown as spheroids embedded in type I collagen and entire spheroids were treated with blue light in the DAPI channel (Leica DMI8 microscope system) in the absence of any further treatment. Cells in target areas were exposed to the following settings: FIM 100%, IL-Fld 2 round, time interval (2 secs), exposure (5 secs), cycle (4 times). Non-irradiated spheroids served as controls (ctrl.). Photoconverted red cells were sorted by FACS and the expression of the indicated genes was assessed by qRT-PCR. Shown are mean ratios with SD of delta-Ct values of UV-treated versus control samples from  $n = 3$  independent experiments performed in triplicates.



**Suppl. Figure 4: Kinetics of LN5-induced ERK1/2 phosphorylation**

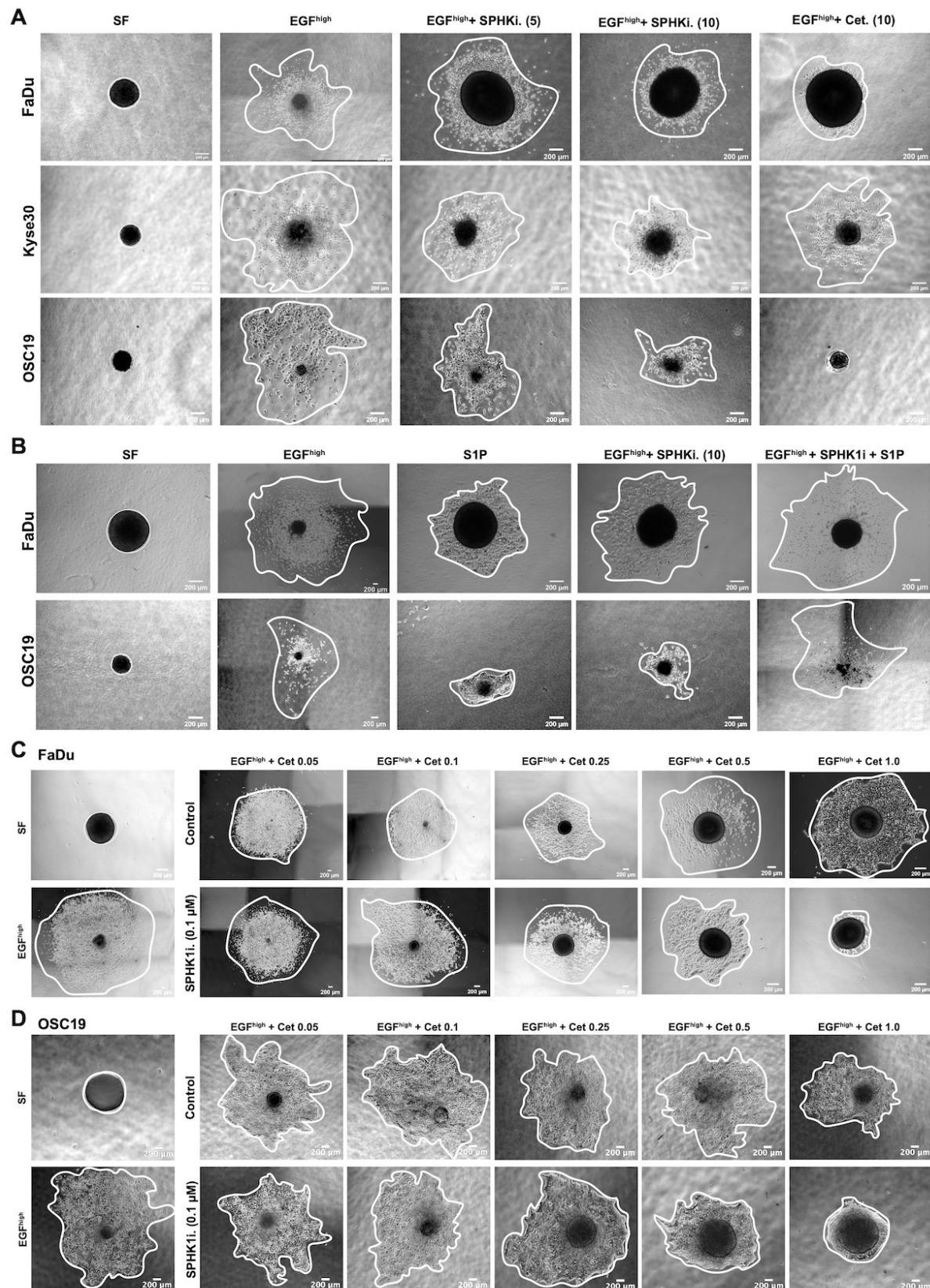
(A-B) FaDu, Kyse30, and Cal27 cells were treated with laminin 5 (LN5) from 0-360 min. Whole cell extracts were separated by immunoblot and phosphorylated ERK (pERK) and ERK1/2 detected with specific antibodies. Shown are representative immunoblots from  $n = 3$  independent experiments in (A). Quantification of  $n = 3$  independent immunoblots as mean with SD and statistical significance is shown in (B). \*  $p$ -value  $< 0.05$ , \*\*  $0.01$ , \*\*\*  $0.001$ , \*\*\*\*  $0.0001$ . (C) FaDu and Cal27 cells were grown as

spheroids, embedded in type I collagen with or without increasing concentrations of laminin 5 (LN5), and treated with EGF as indicated. Shown are representative spheroids after 72 h of treatment with invasive area and distance from  $n = 3$  independent experiments with 5-10 spheroids each per treatment. (D) Quantification of invasive area and distance from  $n = 3$  independent experiments with 5-10 spheroids per treatment. Shown are mean invasive areas and distances with SD for FaDu (left) and Cal27 cells (right). \*\*  $p$ -value  $< 0.01$ , \*\*\*  $< 0.001$ , \*\*\*\*  $< 0.0001$ .



#### Suppl. Figure 5: *ITGB4* knockout in FaDu cells

(A, B, D, and E) *ITGB4* expression was analyzed by flow cytometry in FaDu and Kyse30 wildtype cells (WT) and CRISPR-Cas9-mediated *ITGB4* knockout clones including one *ITGB4*-positive control (*ITGB4*-Ctrl.) and two *ITGB4*-K.O. clones (*ITGB4* KO1 and 2). Shown are representative histograms in (A) and (D) and mean fluorescence intensity (MFI) mean values with SD from  $n = 3$  independent experiments in (B) and (E). (C, F) *ITGB4* expression was analyzed by immunoblotting with specific antibodies in FaDu and Kyse30 WT, *ITGB4*-Ctrl., *ITGB4*-KO1 and -KO2. Shown are representative immunoblots from  $n = 3$  independent experiments for FaDu (C) and Kyse30 (F).

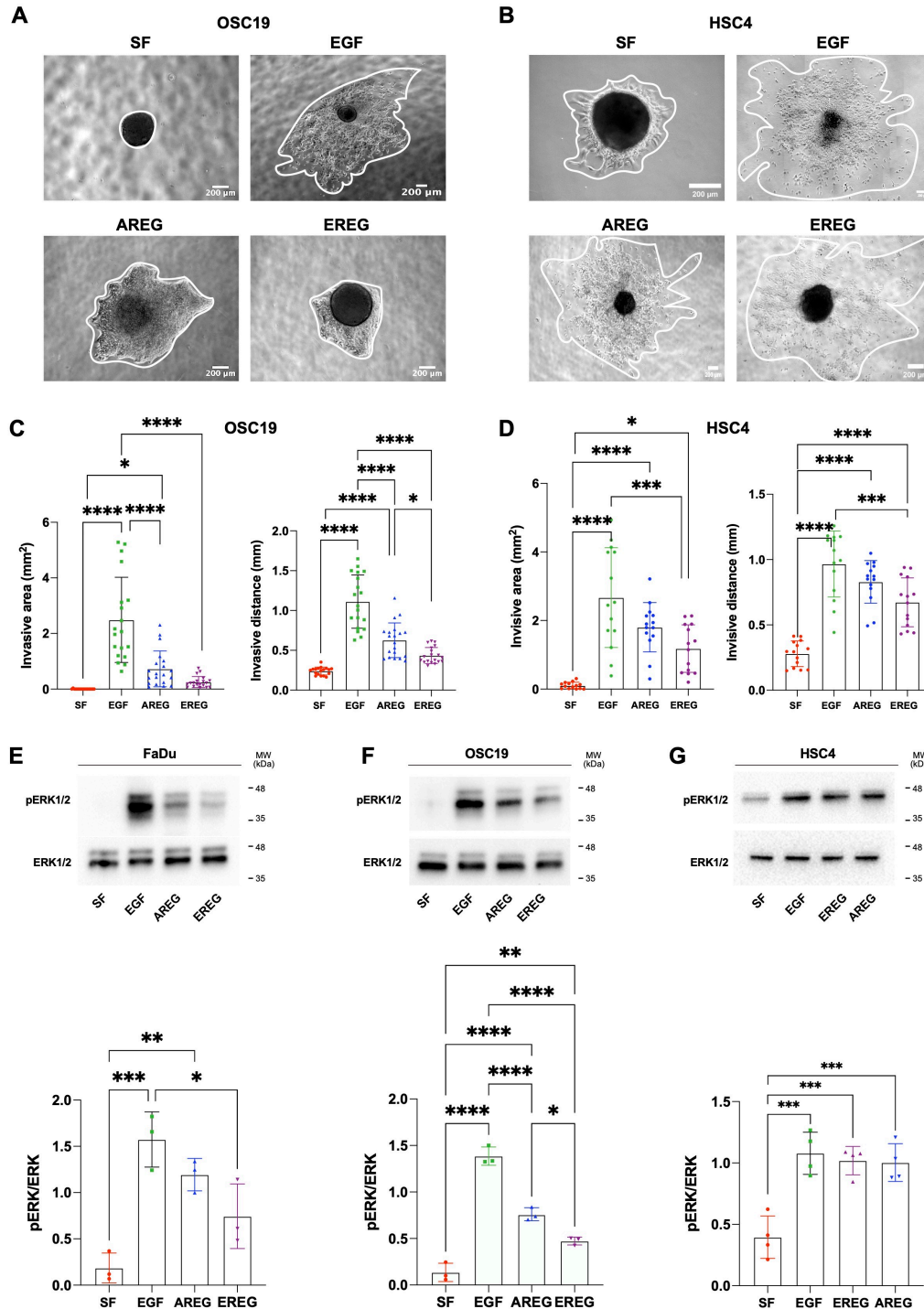


**Suppl. Figure 6: Effects of SPHK1 inhibition on local invasion**

(A) FaDu, Kyse30, and OSC-19 cell spheroids were embedded in type I collagen and treated with EGF (9 nM) in the absence or presence of SPHK1 inhibitor (5 and 10 μg/mL) and Cetuximab (10 μg/mL). Shown are representative pictures from  $n = 3$  independent experiments with 5-10 spheroids per treatment and experiment. (B) FaDu and OSC-19 cell spheroids were embedded in type I collagen and treated with EGF, sphingosine-1-phosphate (S1P), and SPHK1 inhibitor in the indicated combinations.



Shown are representative examples from  $n = 3$  independent experiments performed with 5-10 spheroids for each treatment and experiment. **(C-D)** FaDu (C) and OSC19 spheroids (D) were embedded in type I collagen and treated with EGF in combinations with Cetuximab (0.05-1.0  $\mu\text{g/mL}$ ) and SPHK1 inhibitor (SPHK1i) as indicated. Shown are representative examples from  $n = 3$  independent experiments performed with 5-10 spheroids for each treatment and experiment.

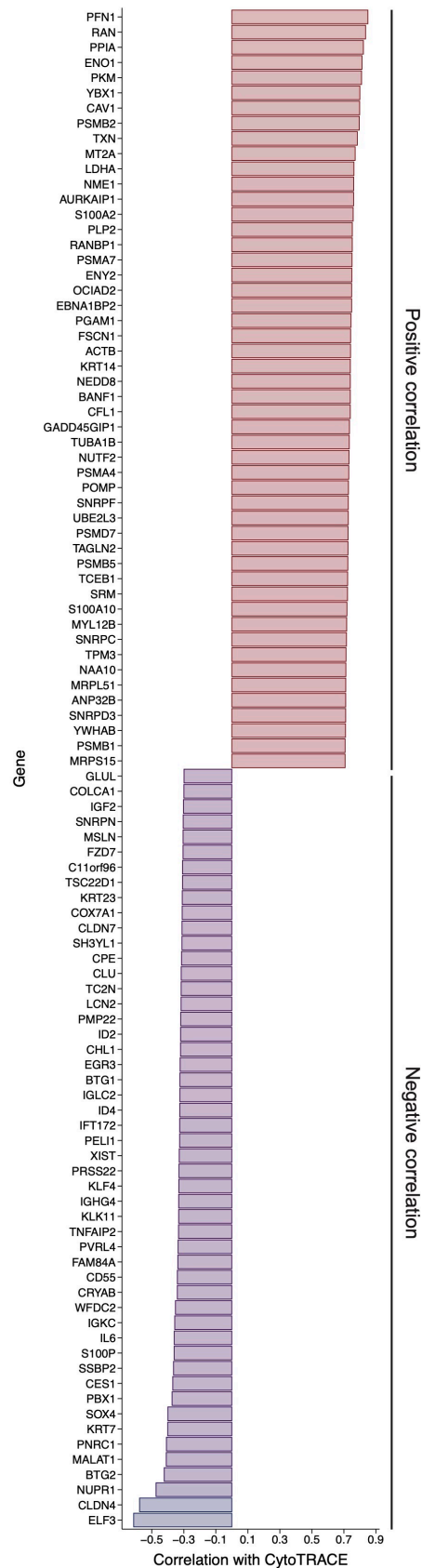


**Suppl. Figure 7: Effects of AREG and EREG on local invasion**

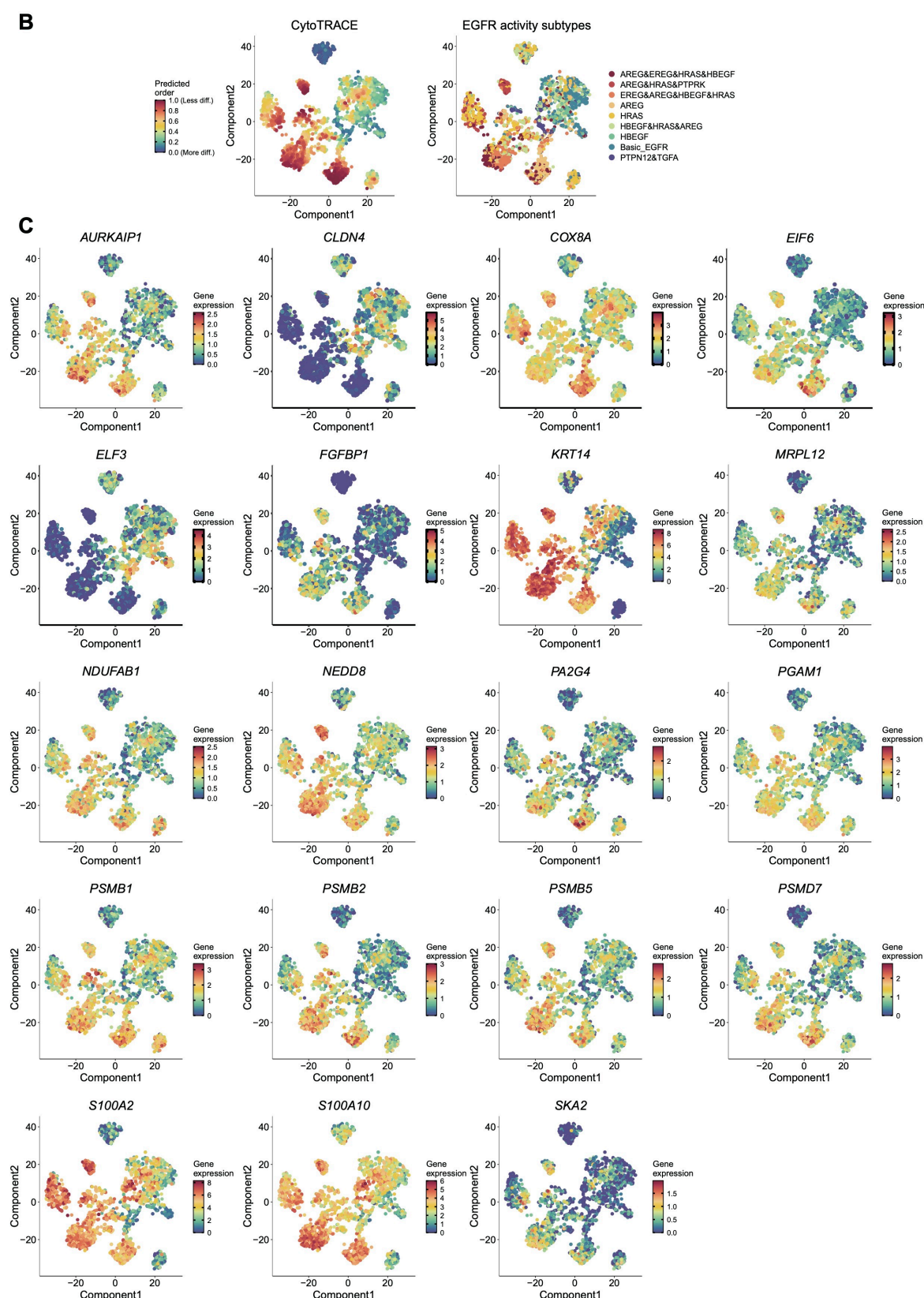
**(A-B)** OSC19 and HSC4 cell spheroids were embedded in type I collagen and treated with EGF (9 nM), AREG (1,000 ng/mL), or EREG (80 ng/mL). Shown are representative pictures from  $n = 3$  independent experiments with 5-10 spheroids per treatment and experiment. **(C-D)** Quantification of invasive area and distance from  $n = 3$  independent experiments with 5-10 spheroids each per treatment. Shown are mean invasive areas and distances with SD for OSC19 (C) and HSC4 cells (D). **(E-G)** FaDu (E), OSC19 (F), and HSC4 cells (G) were treated in monolayer cultures with EGF (9 nM), AREG (1,000 ng/mL), or

EREG (80 ng/mL) under serum-free conditions (10 min). Phosphorylated and total levels of ERK1/2 were visualized by immunoblotting with specific antibodies. Shown are representative immunoblots (top) and quantifications as mean with SD from  $n = 3$  independent experiments (bottom). \*  $p$ -value  $< 0.05$ , \*\*\*\*  $< 0.0001$ .

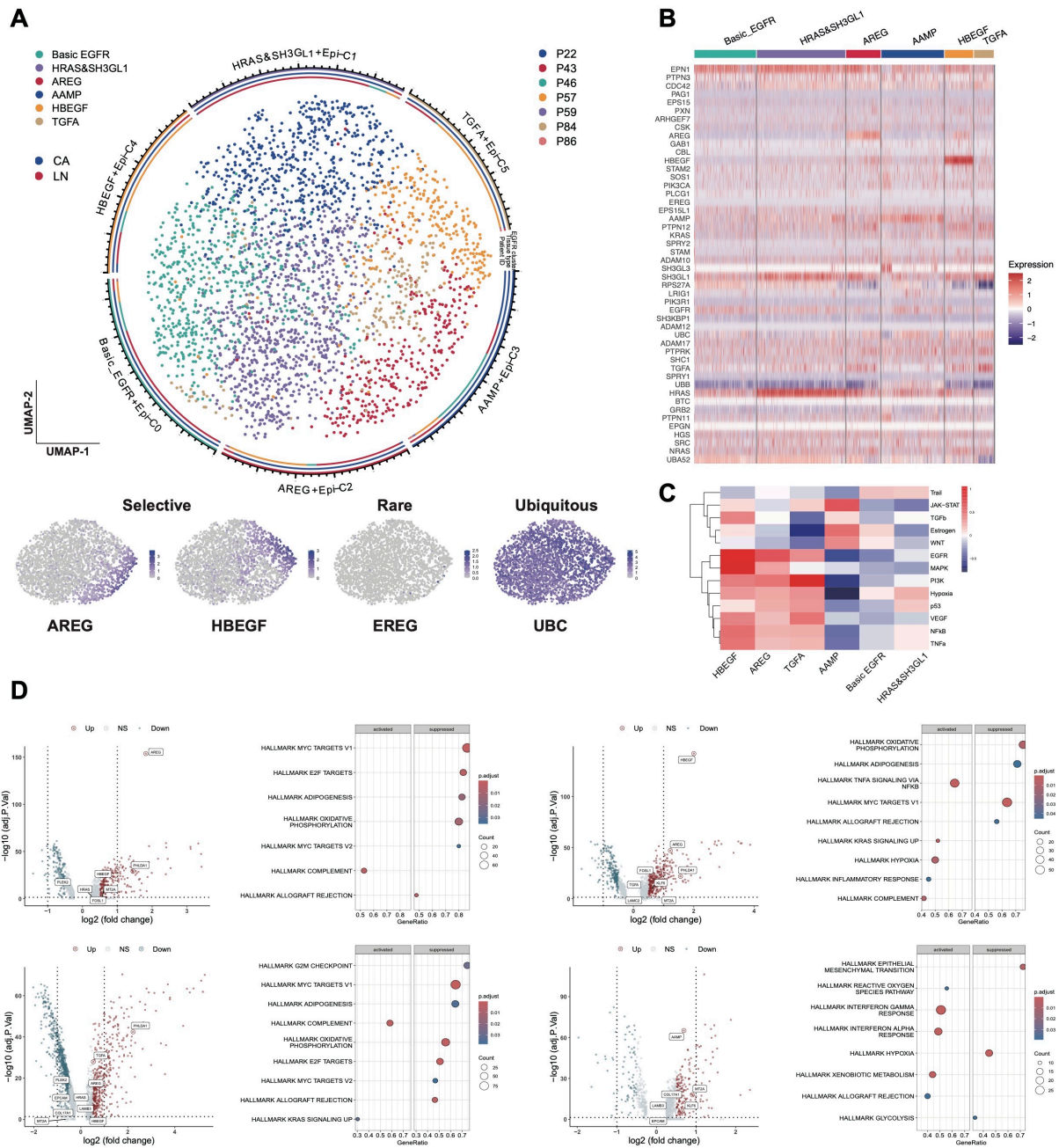
**A**





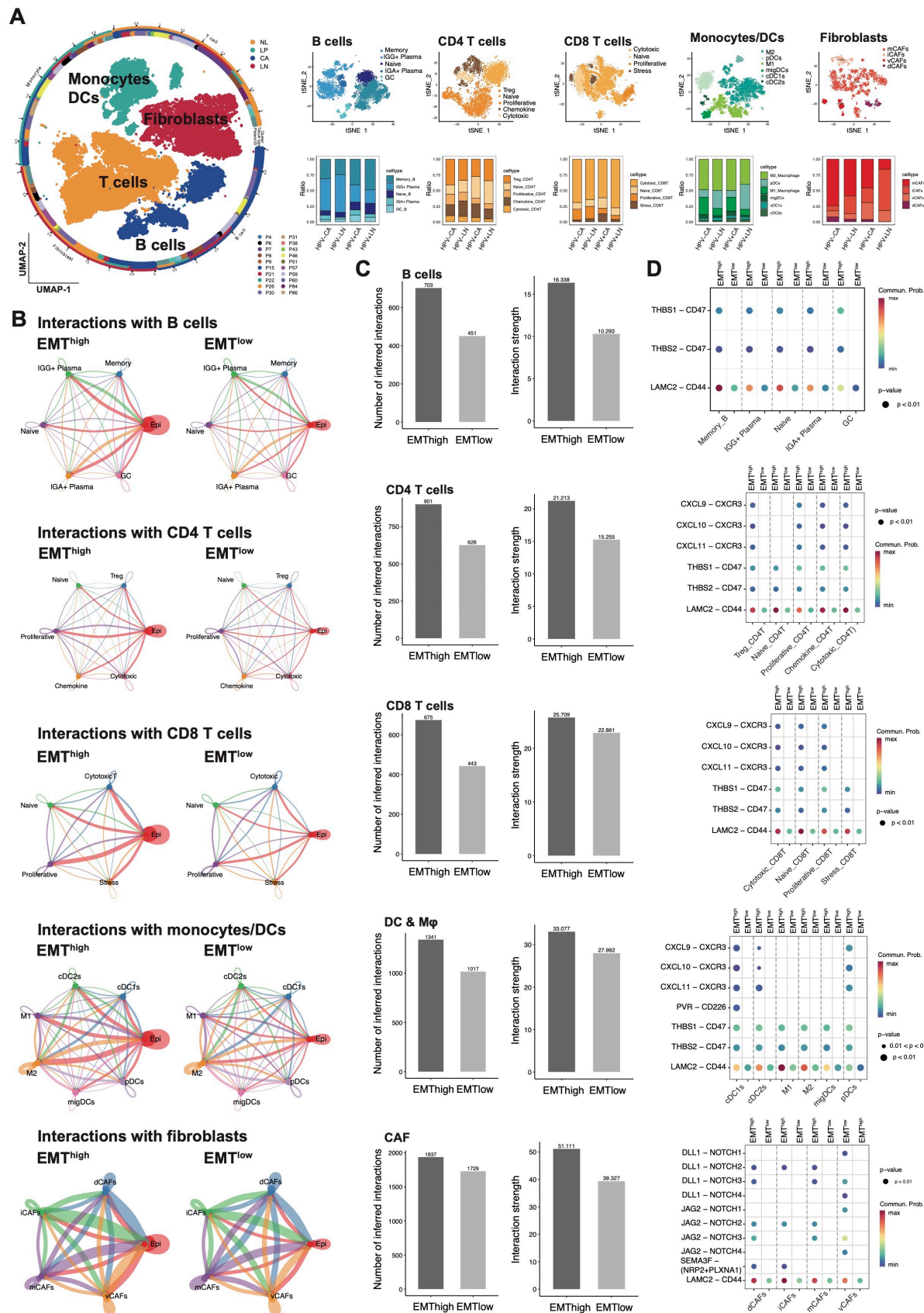


**Suppl. Figure 8: Expression of CytoTRACE differentiation score-associated genes in GSE181919** (A) Shown are the top  $n = 50$  genes positively and the top  $n = 50$  genes negatively correlated with the CytoTRACE score in malignant epithelial cells of GSE181919 (Pearson). (B) UMAP representation of CytoTRACE differentiation scores (left) and EGFR-activity subtypes (right) in malignant epithelial cells of GSE181919. Shown is the predicted order from more to less differentiated and all EGFR-activity subtypes by color-coding. (C) UMAP representation of  $n = 19$  genes associated with high CytoTRACE scores from GSE181919 that are significantly correlated to OS in HPV-neg. HNSCC-TCGA samples.



### Suppl. Figure 9: Identification of EGFR-activity subtypes in HPV-pos. HNSCC

(A) EGFR-activity subtypes identified by non-negative matrix factorization (NMF) from HPV-pos. malignant HNSCC cells (primary tumor and nodal metastases) are depicted in a UMAP with tissue type of origin and patient ID. Examples of selective genes (AREG, HBEGF), rare genes (EREG), and ubiquitous genes (UBC) are depicted in the lower UMAPs. (B) Heatmap representation of the gene expression of “REACTOME\_SIGNALING\_BY\_EGFR” in EGFR-activity subtypes. (C) Heatmap of intensity scores of  $n = 13$  PROGENY signaling pathways for all EGFR-activity subtypes of HPV-pos. malignant cells. (D) Volcano plots with  $\log_2FC$  and  $p$ -value of DEGs from “AREG” versus “Basic EGFR” subtypes and “HBEGF” versus “Basic EGFR” subtypes are shown. Gene set variation analysis (GSVA) of “AREG” versus “Basic EGFR” and “HBEGF” versus “Basic EGFR” are presented (right panels). Shown are significantly activated and suppressed human cancer hallmarks (MSigDB) with gene counts and adjusted  $p$ -values.



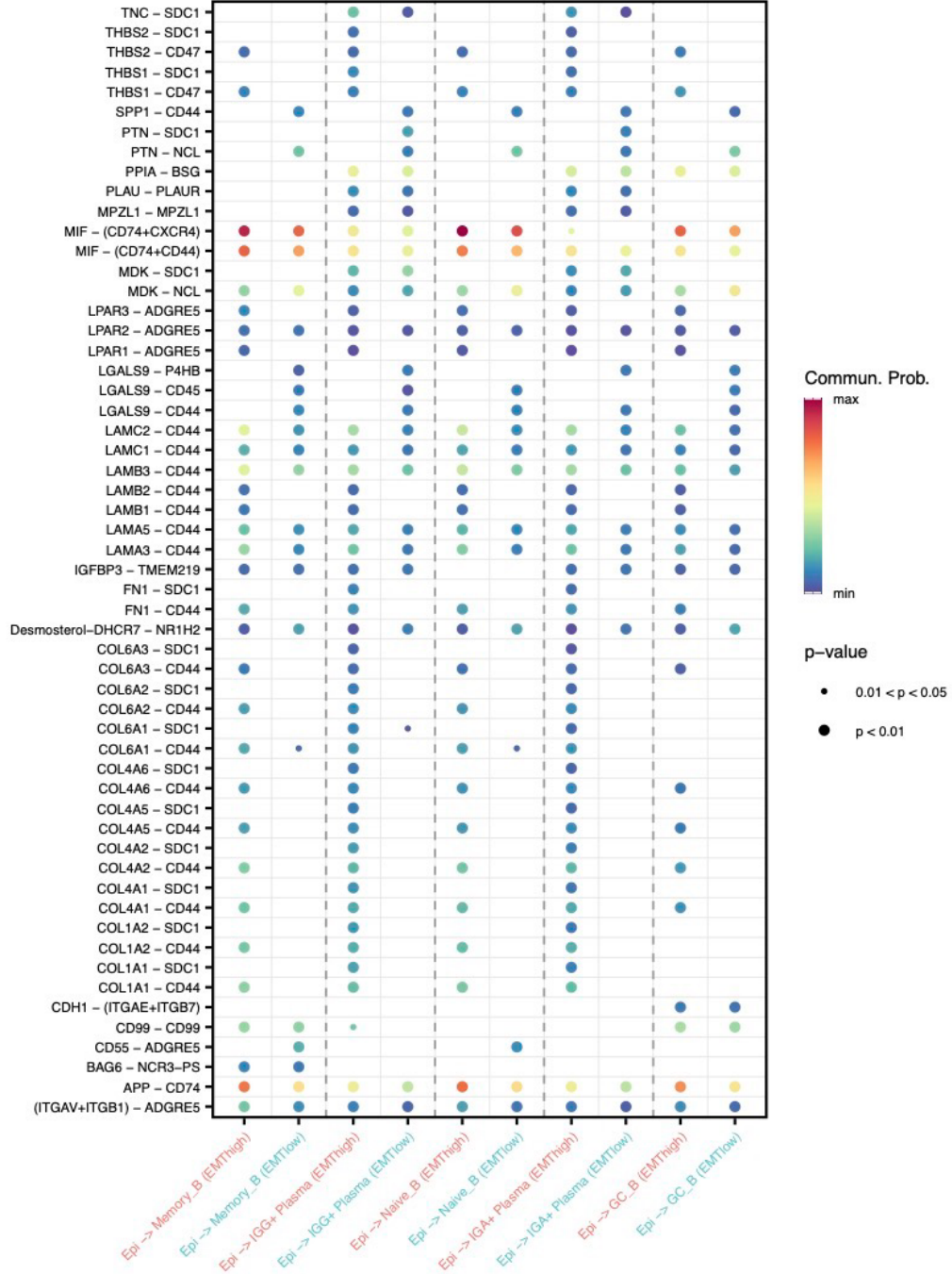
**Suppl. Figure 10: EMT<sup>high</sup>-associated EGFR-activity subtypes interactions with non-malignant cells**

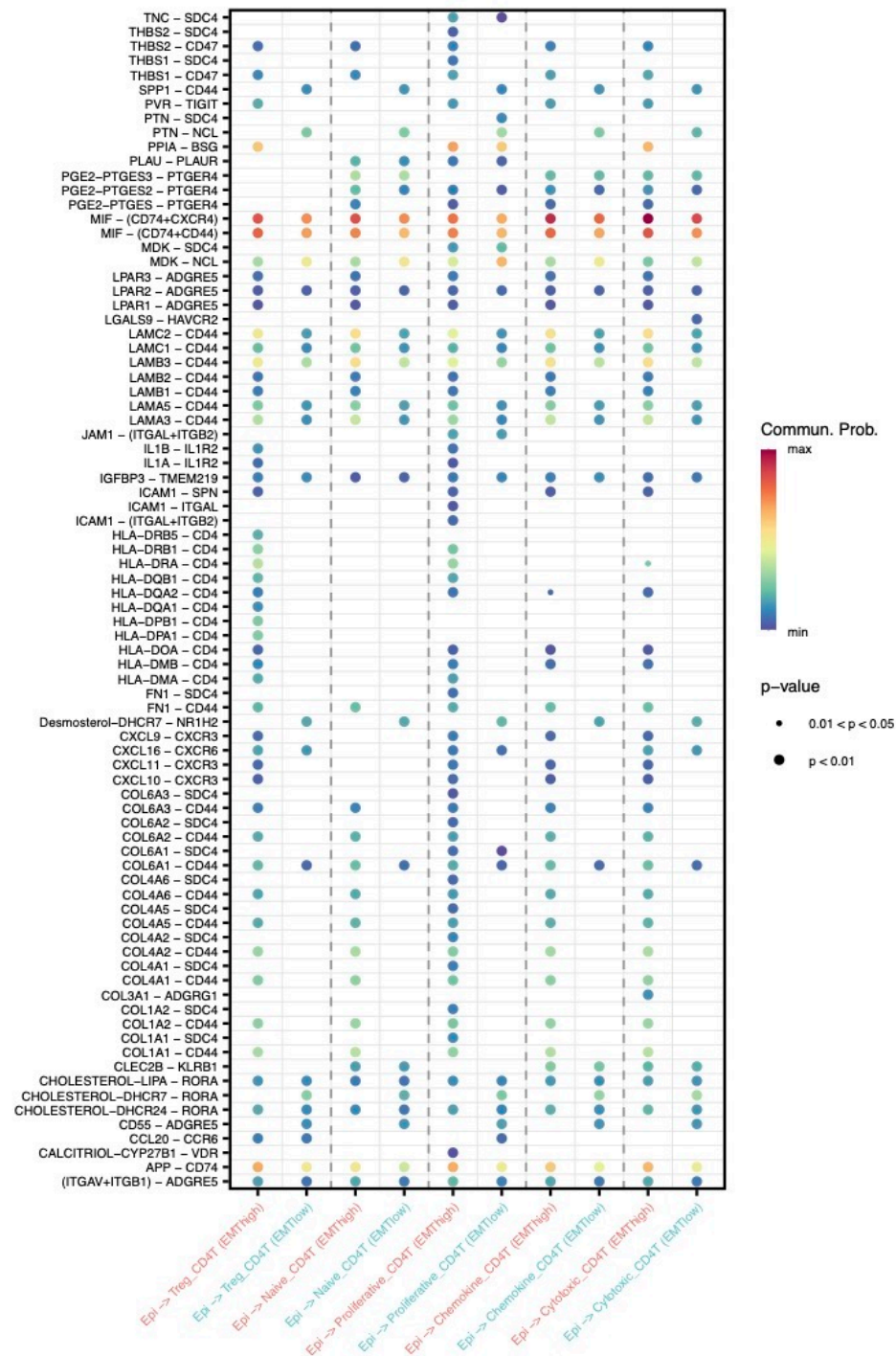
(A) B cells, CD4 and CD8 T cells, monocytes, dendritic cells, and fibroblasts were annotated in GSE181919. Shown are UMAP representations of all immune and stromal cells (left), and single UMAP representations for each cell subtype with stacked bar graphs of proportions of B cells, CD4 and CD8 T cells, monocytes, dendritic cells, and fibroblast subtypes, as indicated (right). (B) Interactions of



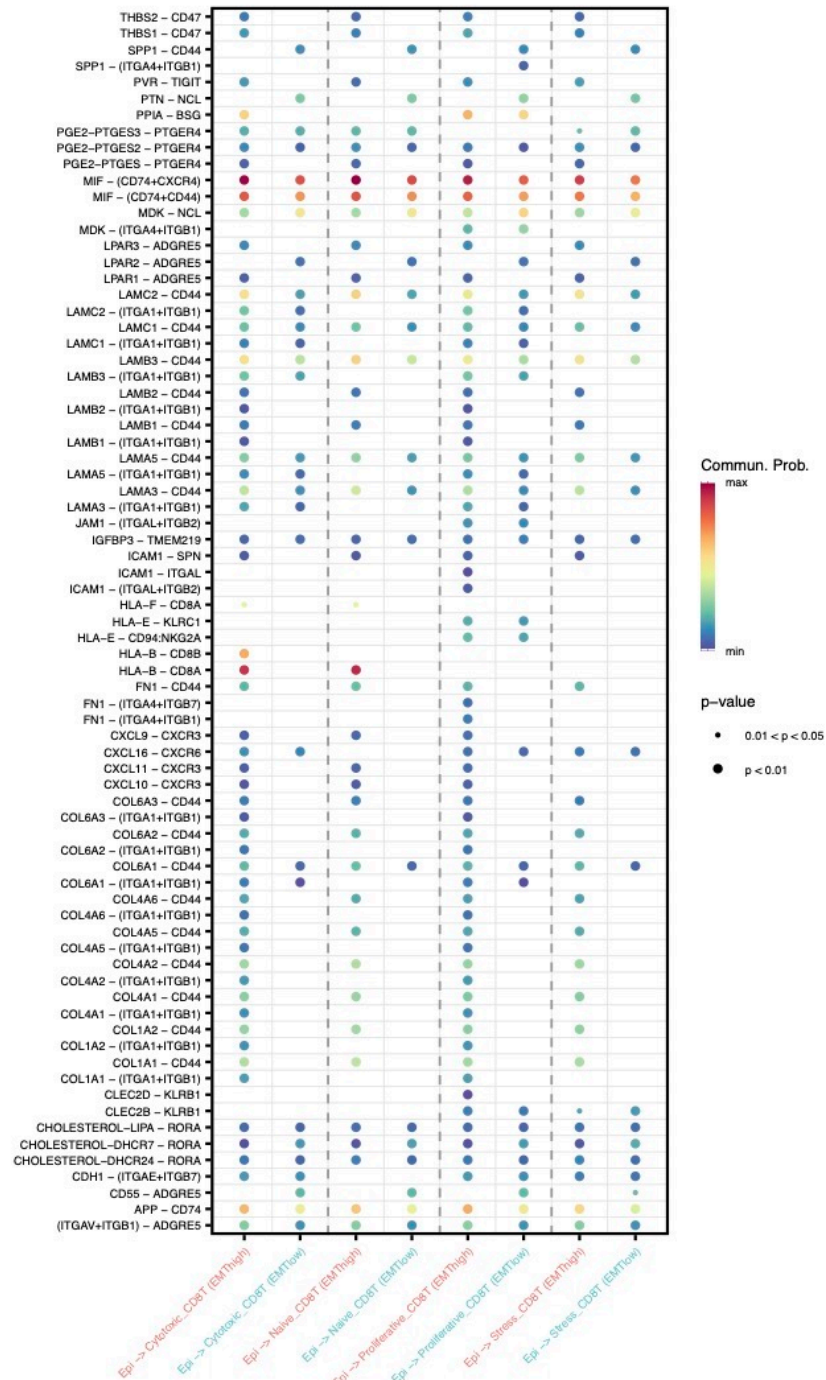
malignant cells with highest EMT scores (EMT<sup>high</sup>, “AREG&HRAS&PTPRK” subtype) and lowest EMT scores (EMT<sup>low</sup>, “Basic EGFR” subtype) with B cells, CD4 and CD8 T cells, monocytes, dendritic cells, and fibroblast subtypes are shown. **(C)** Numbers and interaction strength of EMT<sup>high</sup> and EMT<sup>low</sup> malignant cells with B cells, CD4 and CD8 T cells, monocytes, dendritic cells, and fibroblasts are shown as bar graphs. **(D)** Selective ligand-receptor interactions of EMT<sup>high</sup> and EMT<sup>low</sup> malignant cells with B cells, CD4 and CD8 T cells, monocytes, dendritic cells, and fibroblasts are shown as dot plots, with communication probabilities, p-values, and LAMC-CD44 interactions as reference. First gene = malignant cells, second gene = non-malignant cells.

## A Interactions with B cells



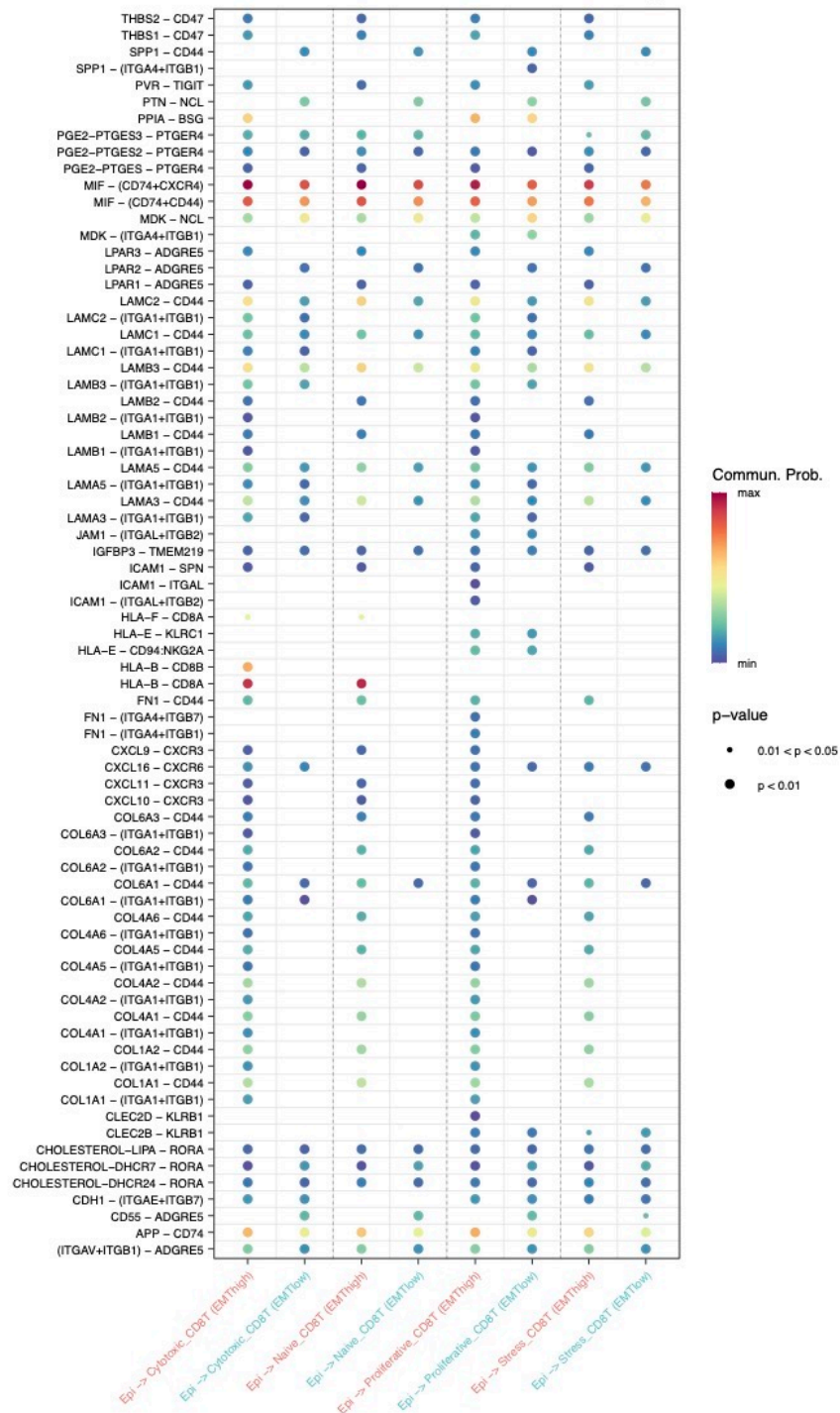
**B****Interactions with CD4 T cells**

# C Interactions with CD8 T cells

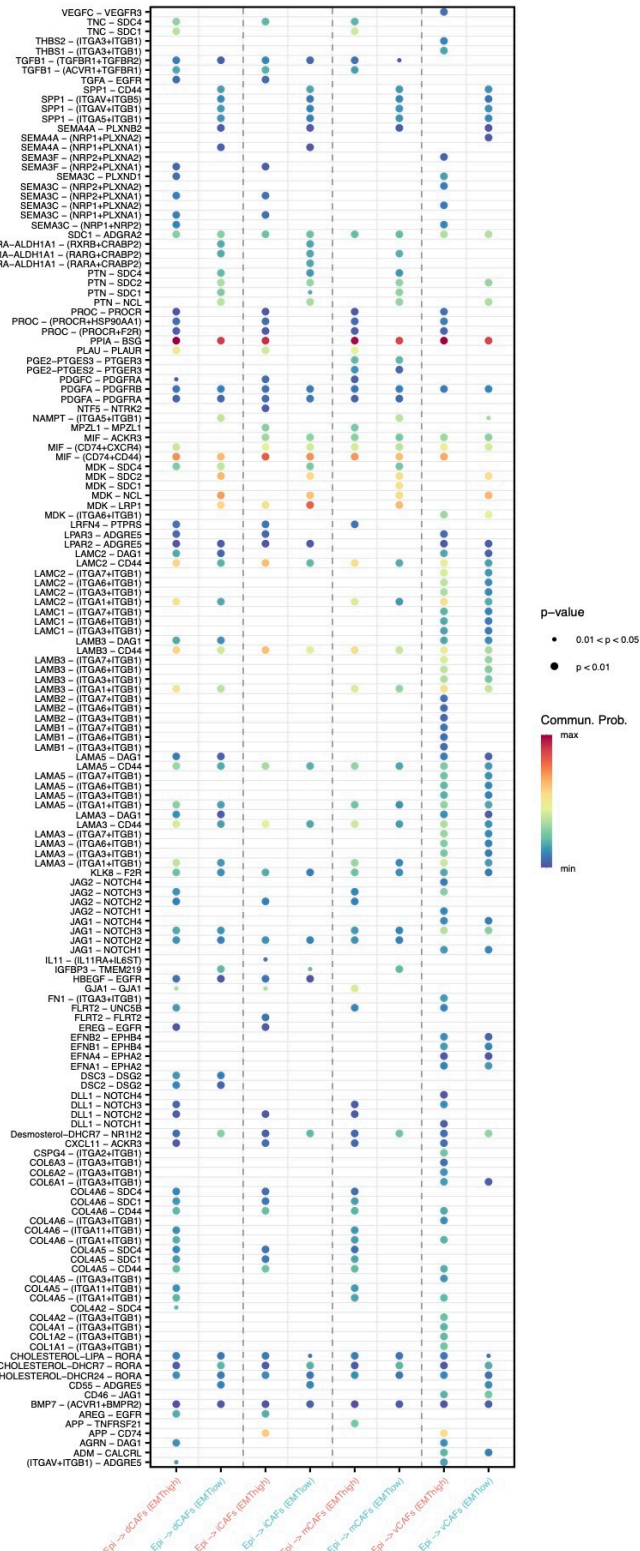




# D Interactions with monocytes/DCs

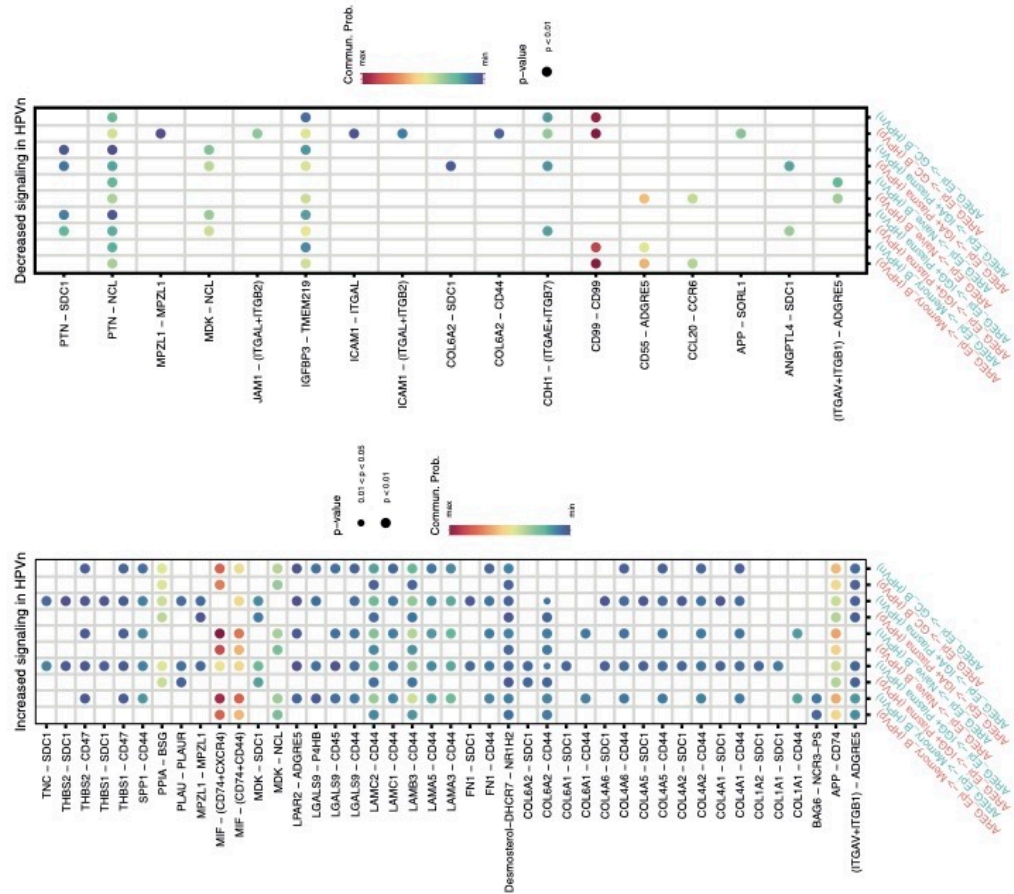
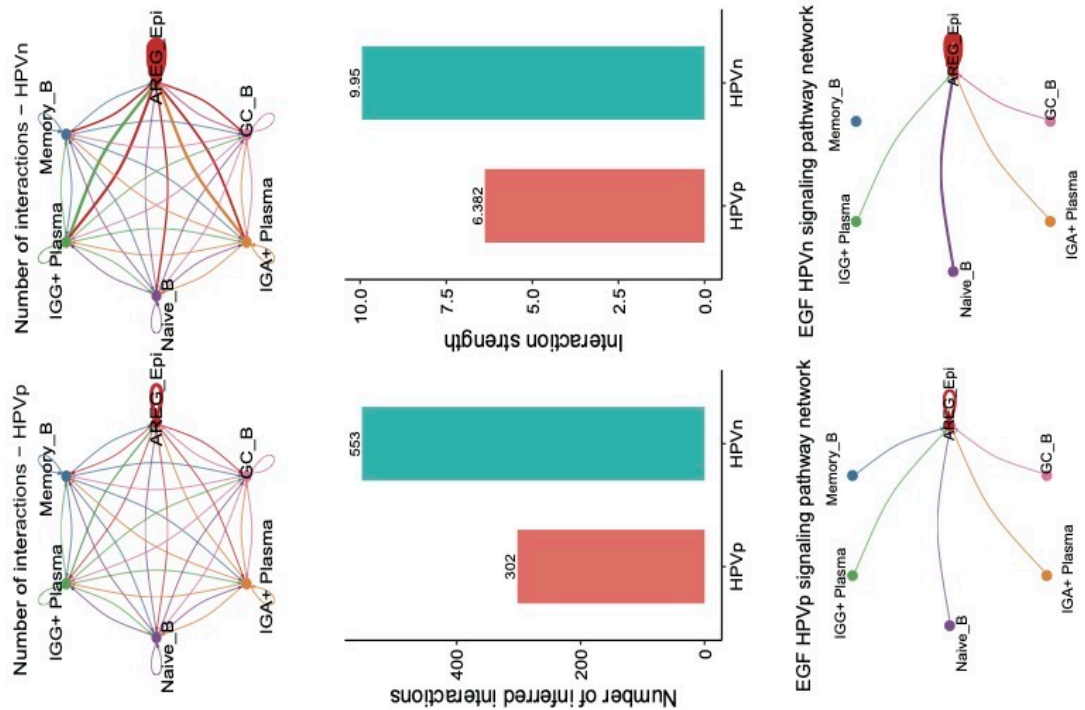


## E Interactions with fibroblasts



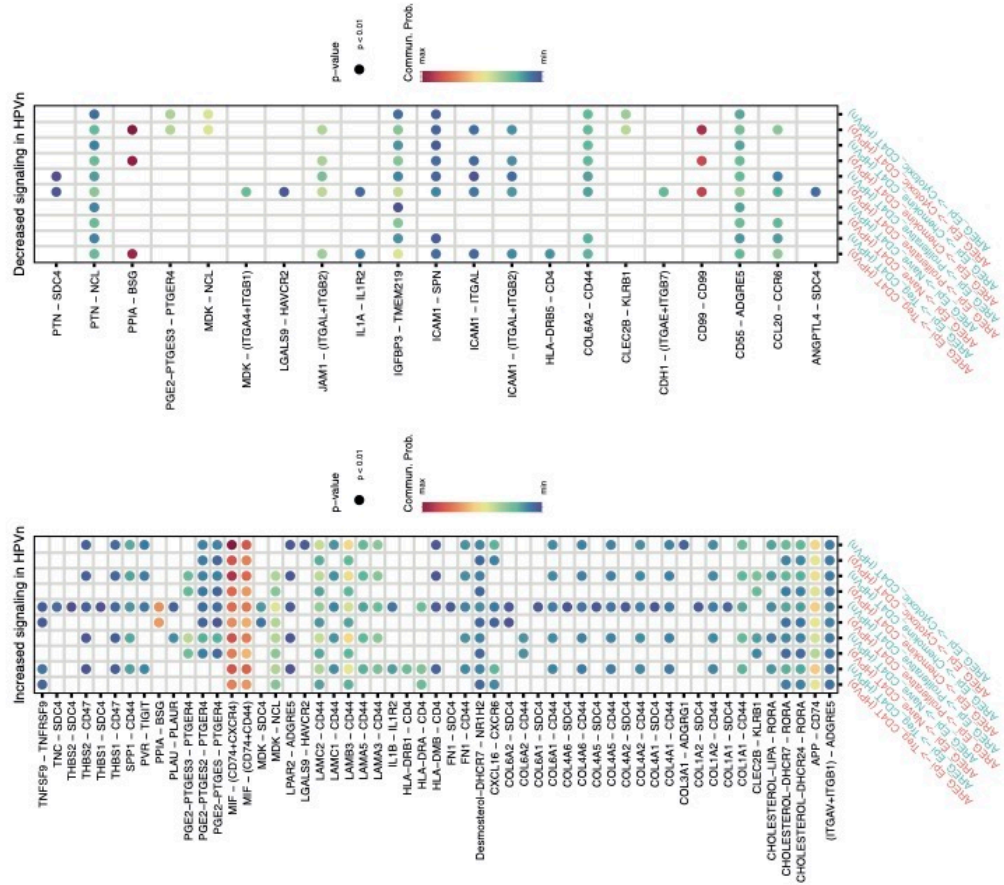
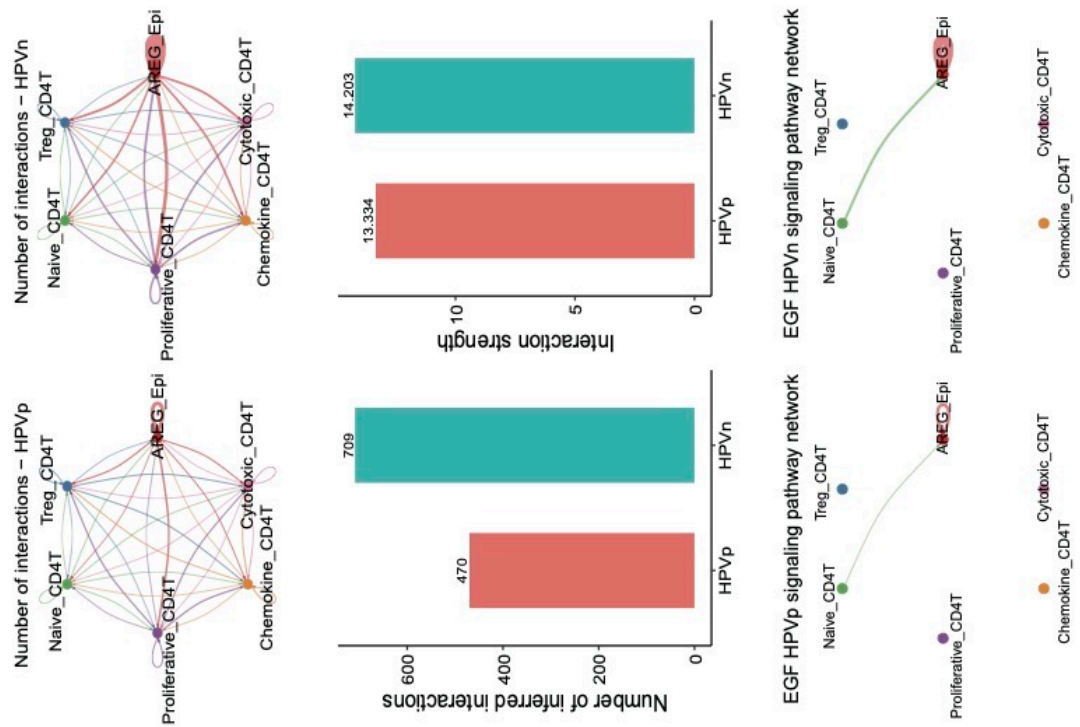
**Suppl. Figure 11: Ligand-receptor interactions of EMT<sup>high</sup> and EMT<sup>low</sup> malignant cells with non-malignant cells**

All ligand-receptor interactions of EMT<sup>high</sup> and EMT<sup>low</sup> malignant cells (GSE181919) with B cells (A), CD4 and CD8 T cells (B, C), monocytes and dendritic cells (D), and fibroblasts (E) are shown as dot plots, with communication probabilities, and p-values. First gene = malignant cells, second gene = non-malignant cells.

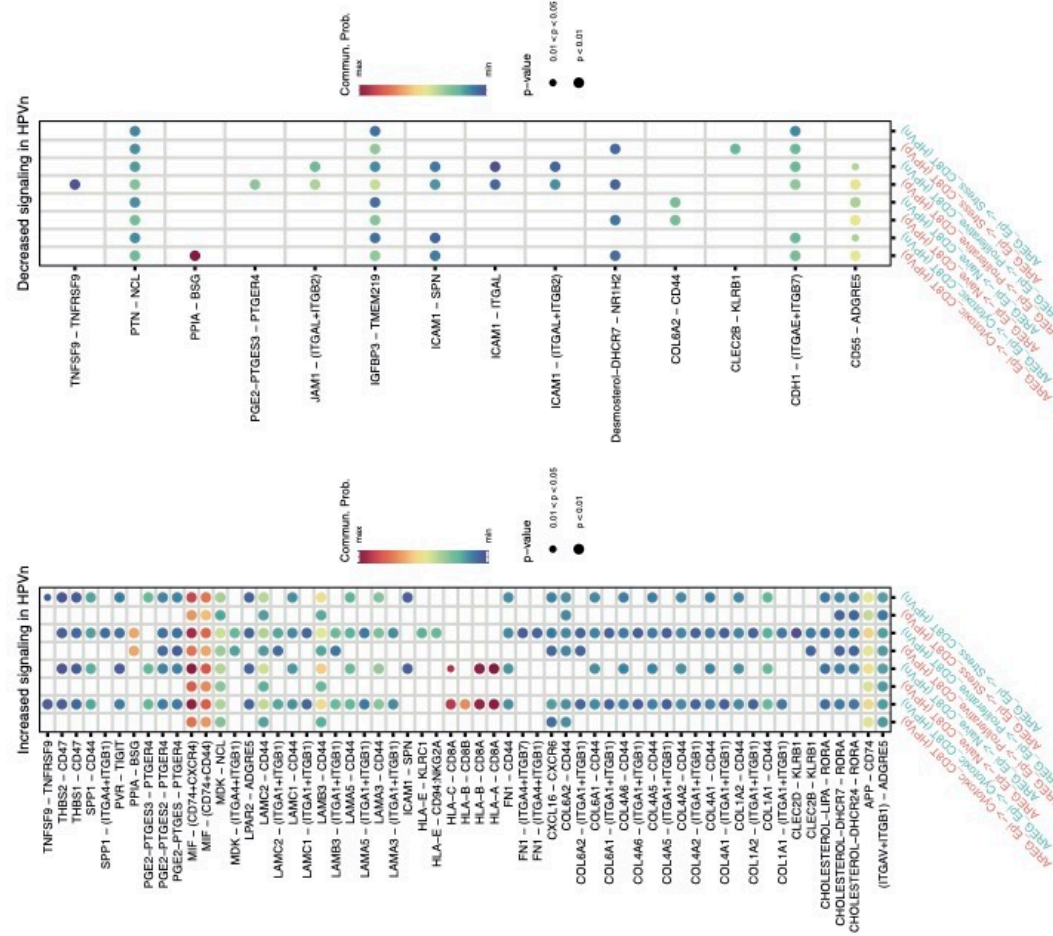
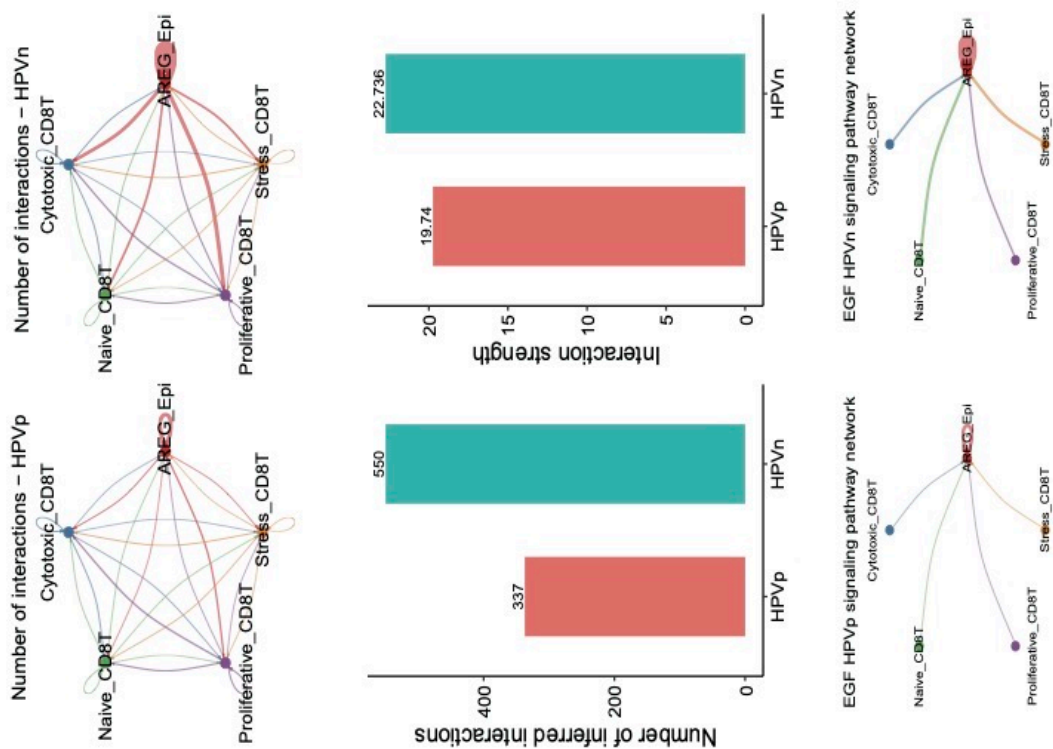




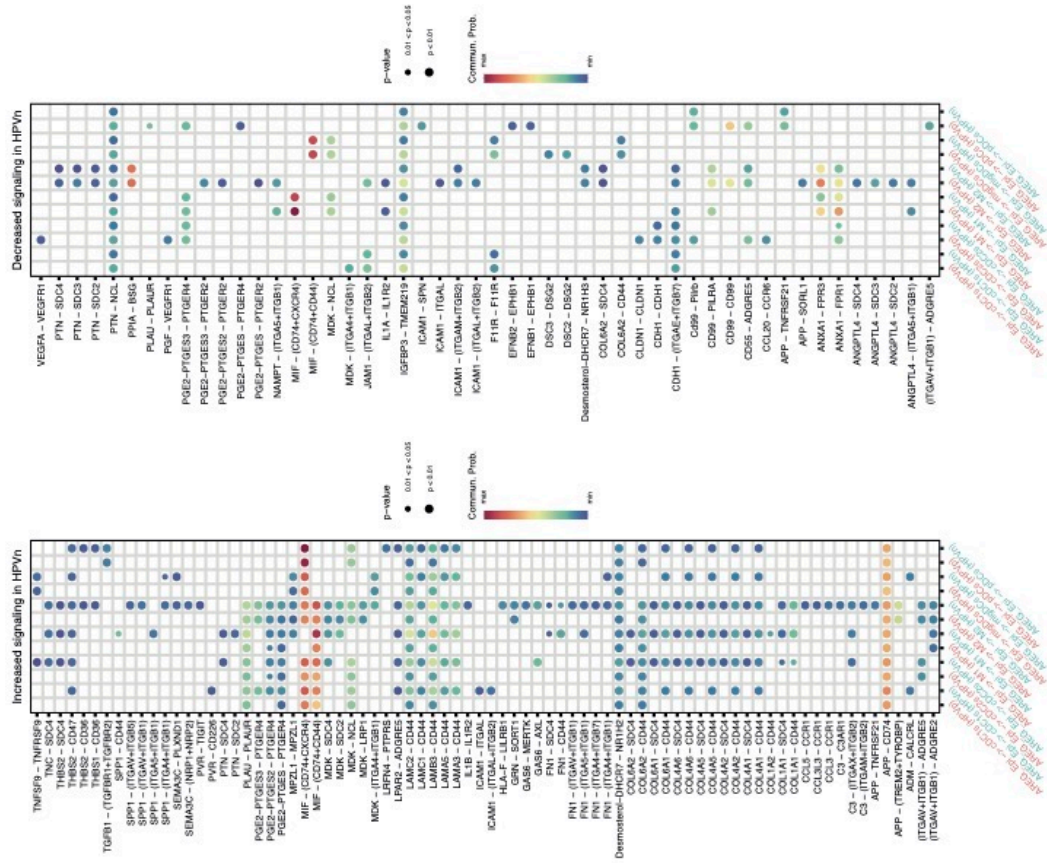
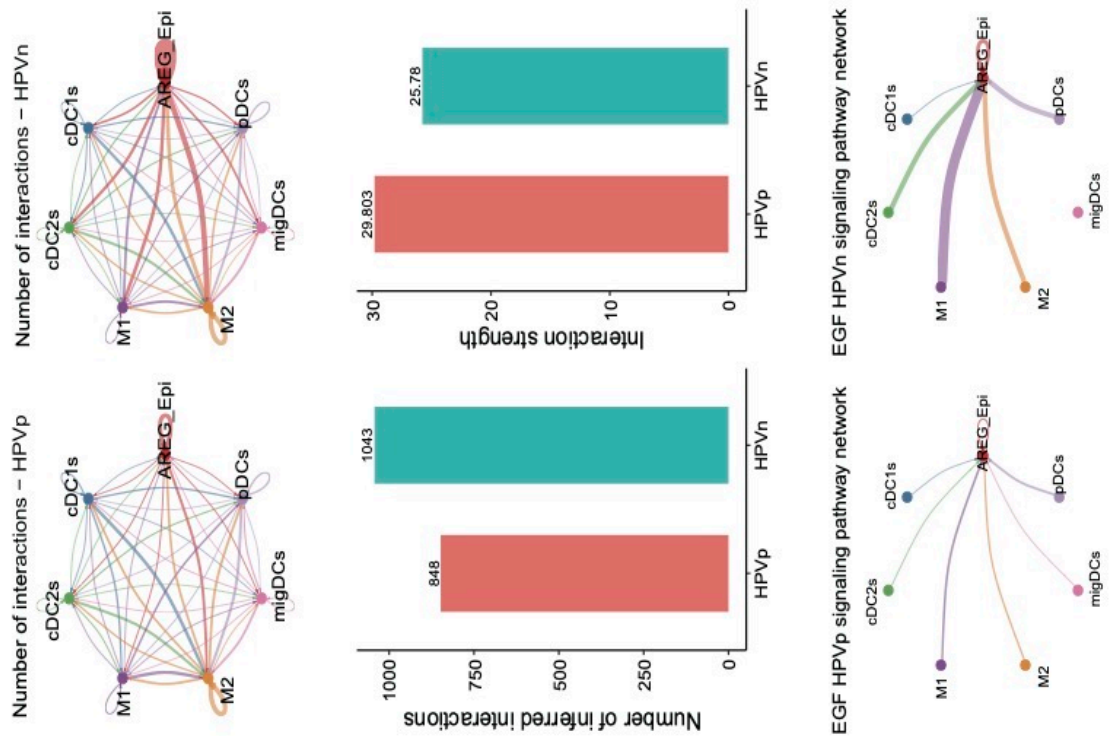
**B**



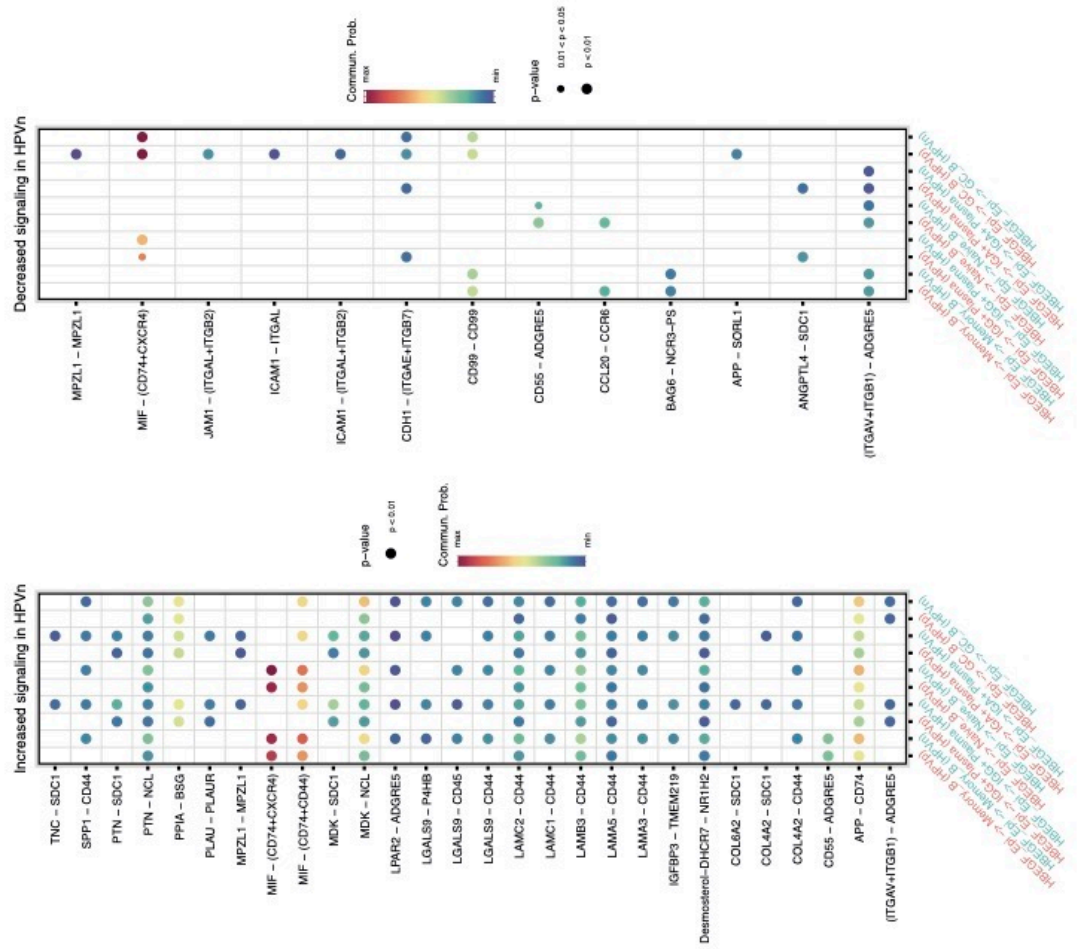
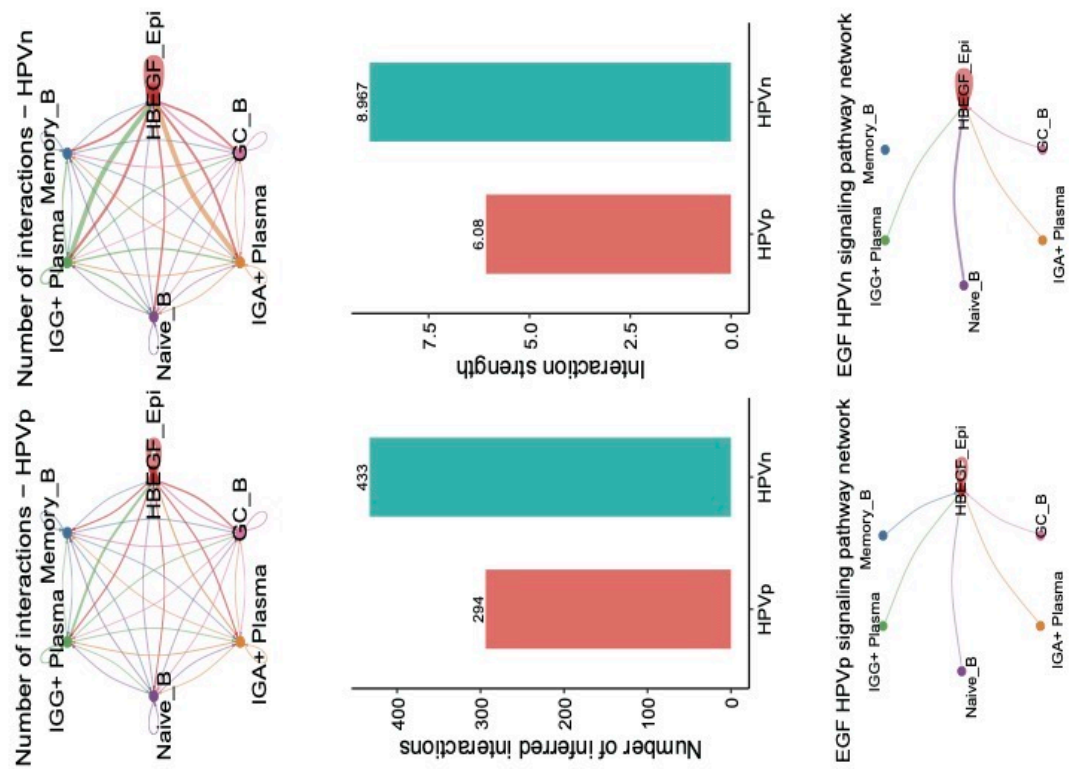
C

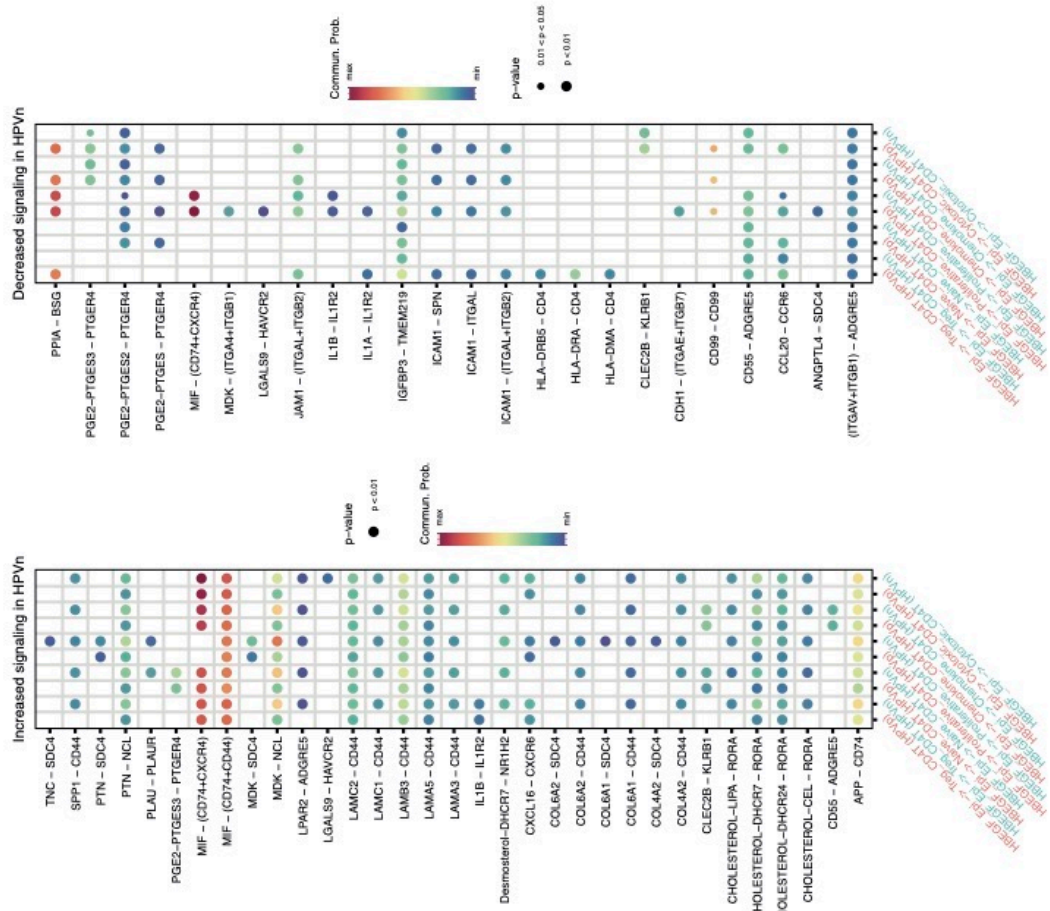
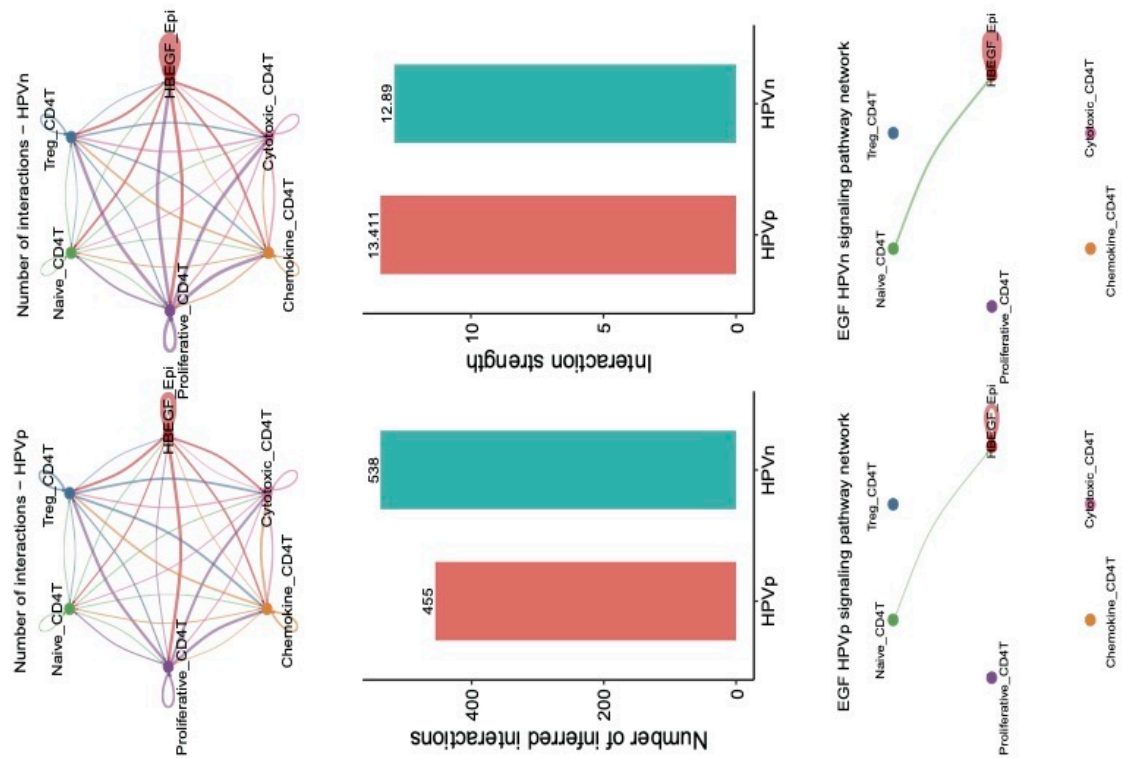


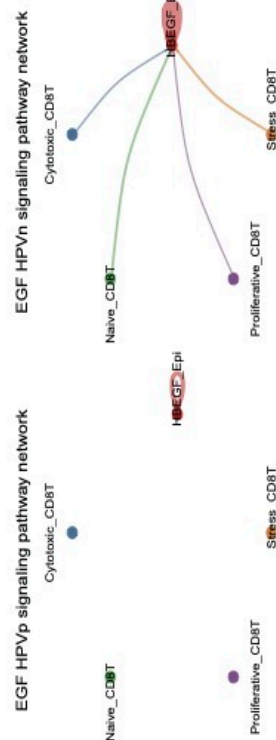
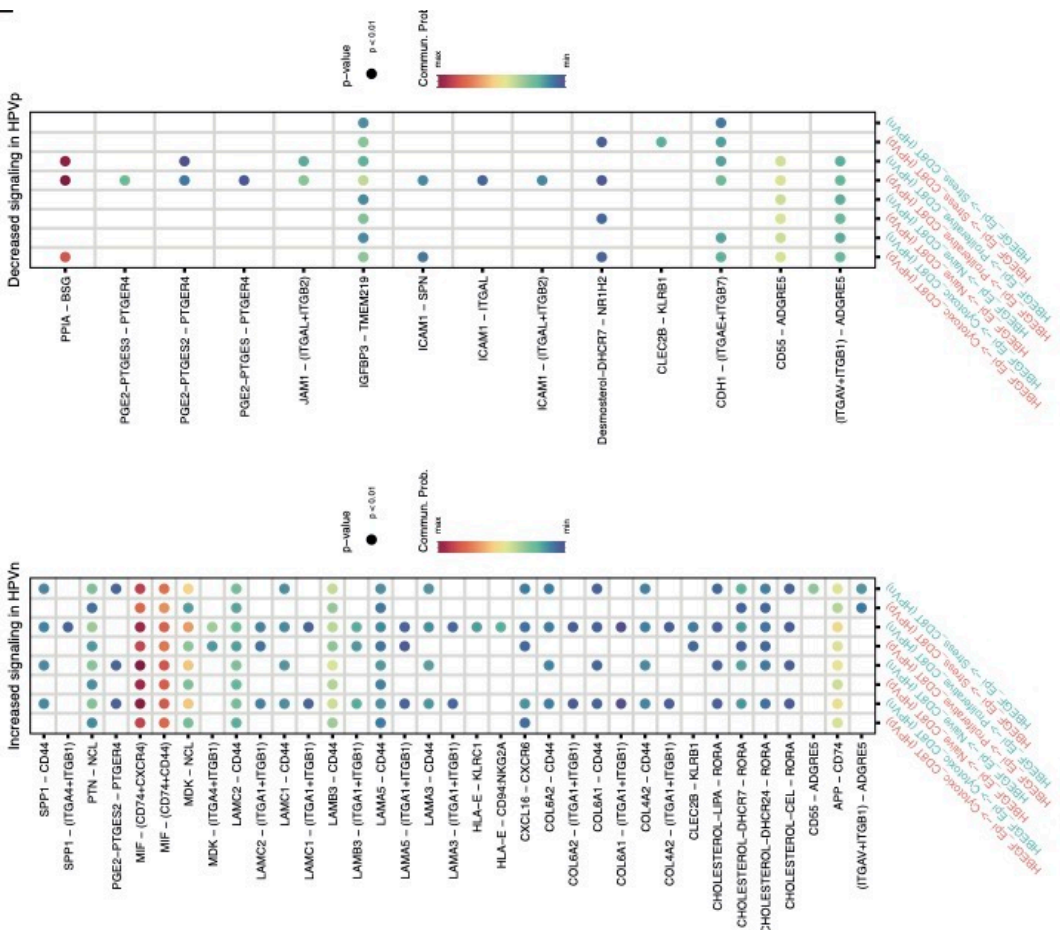
D



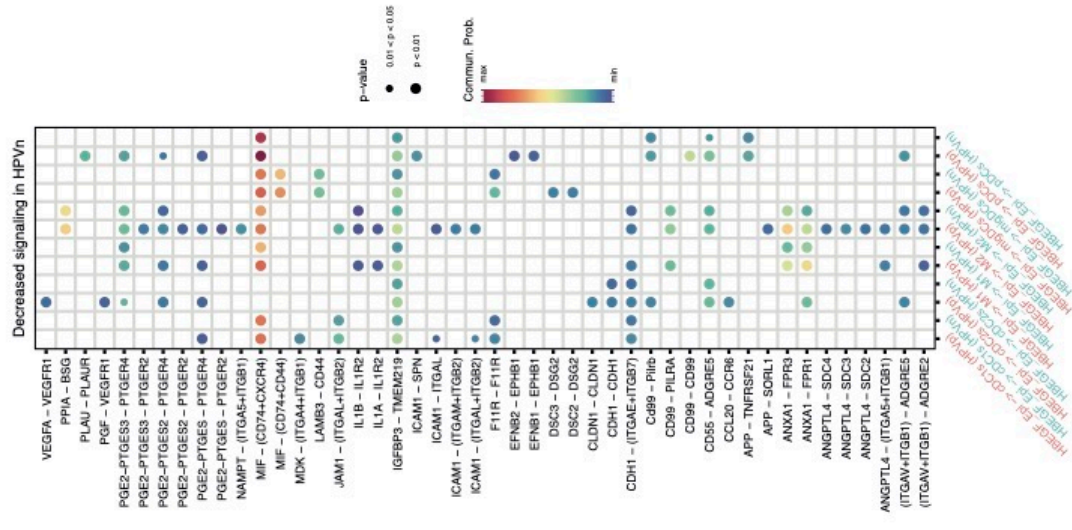
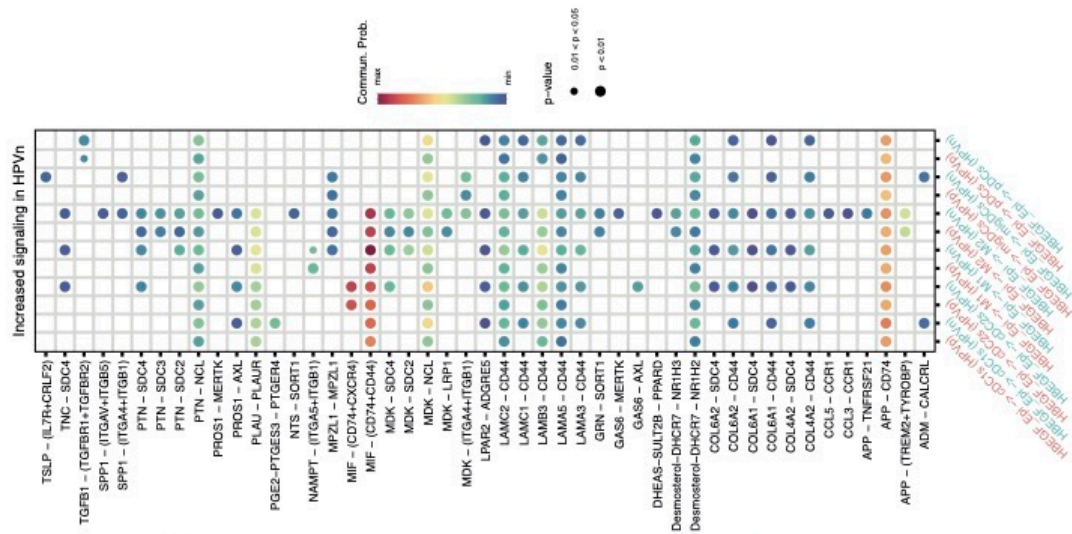
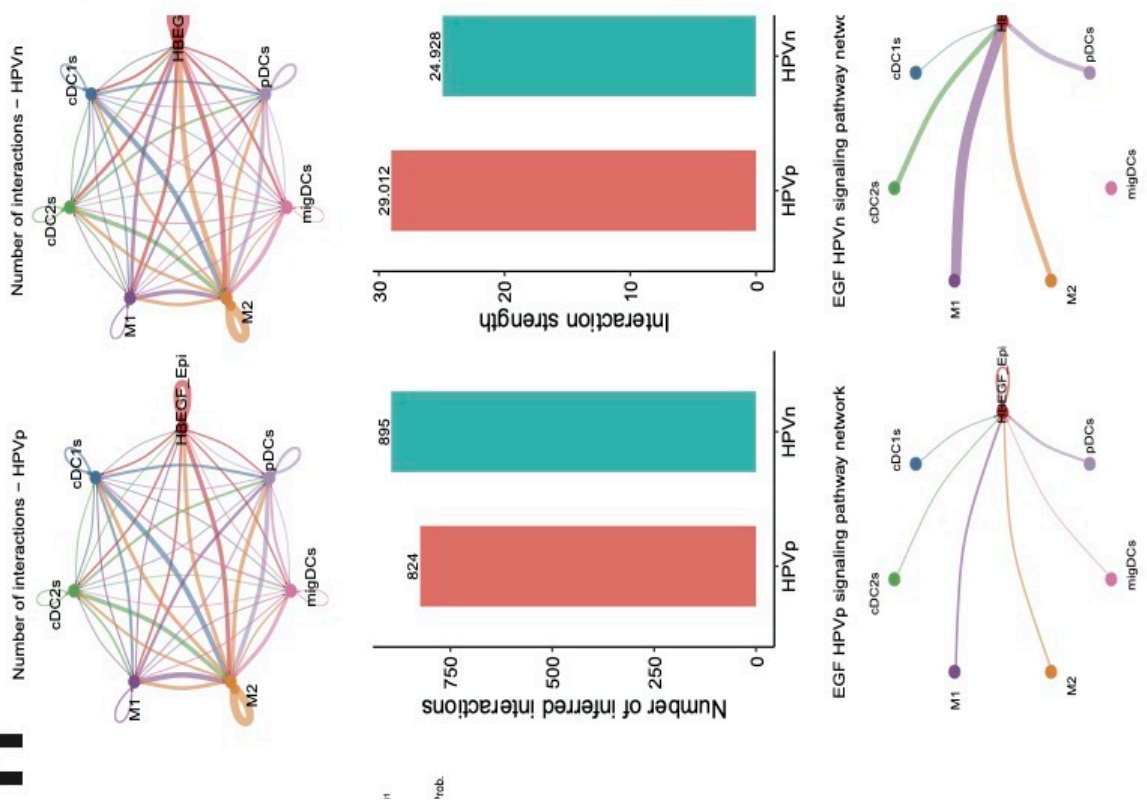


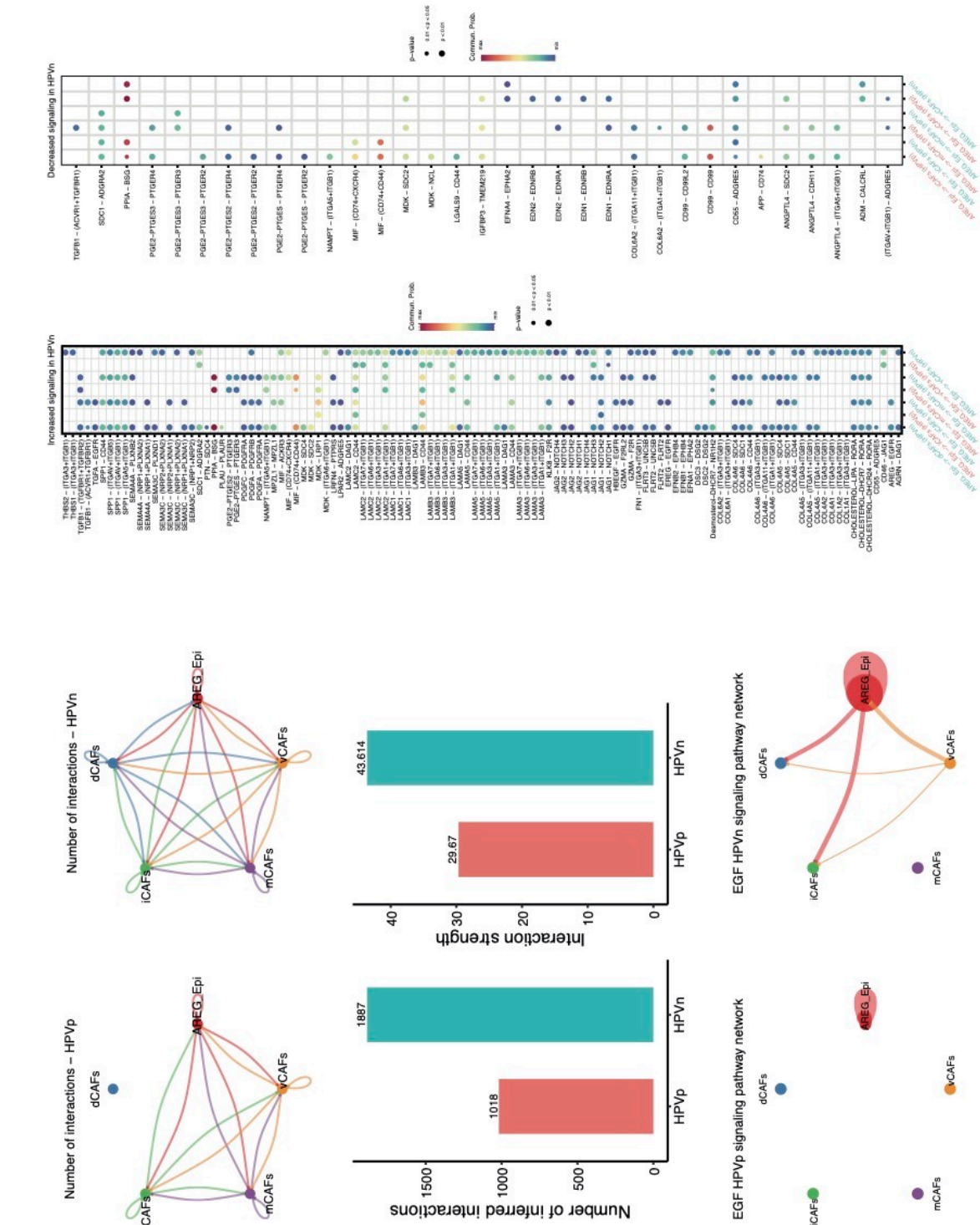


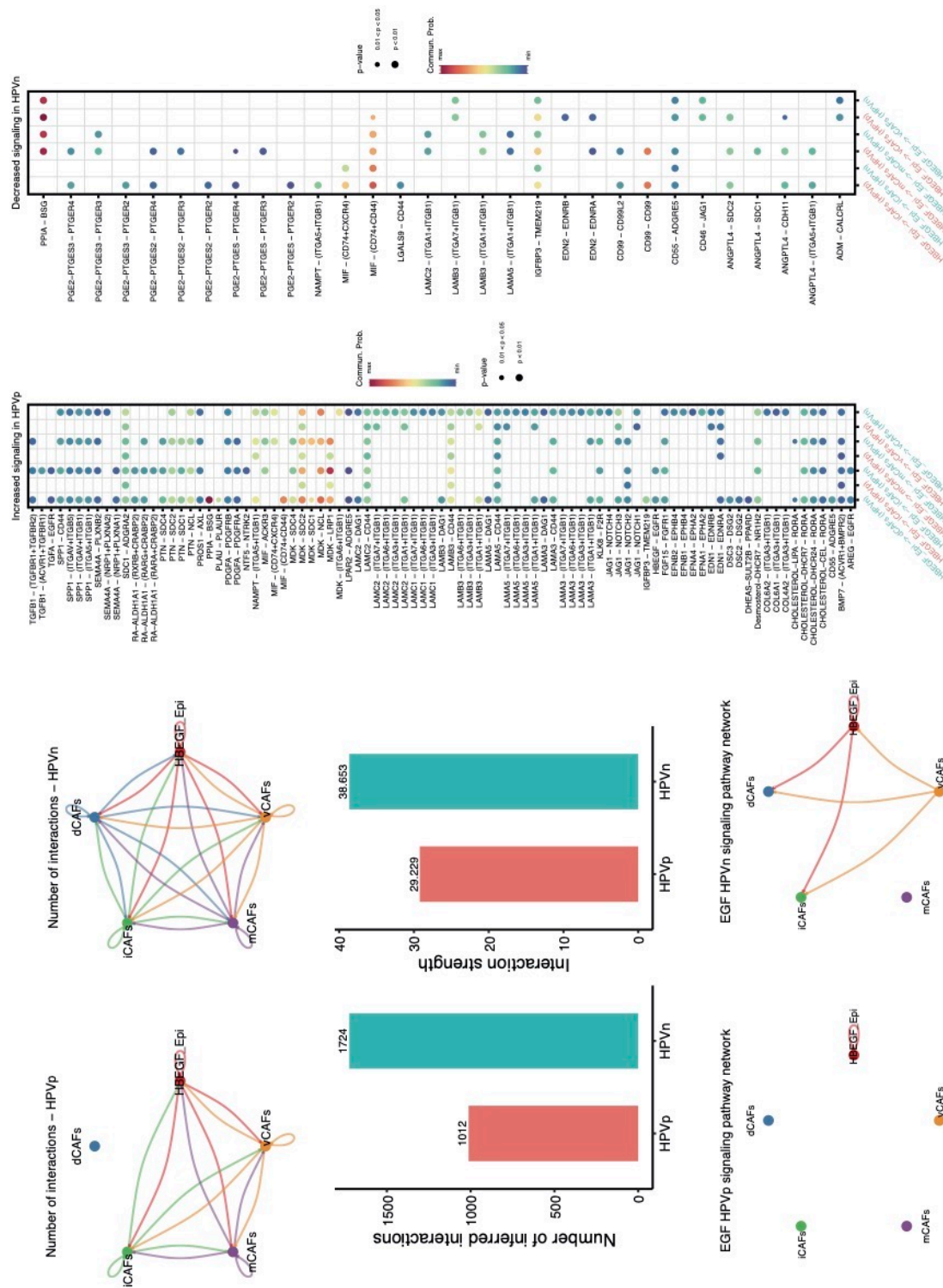








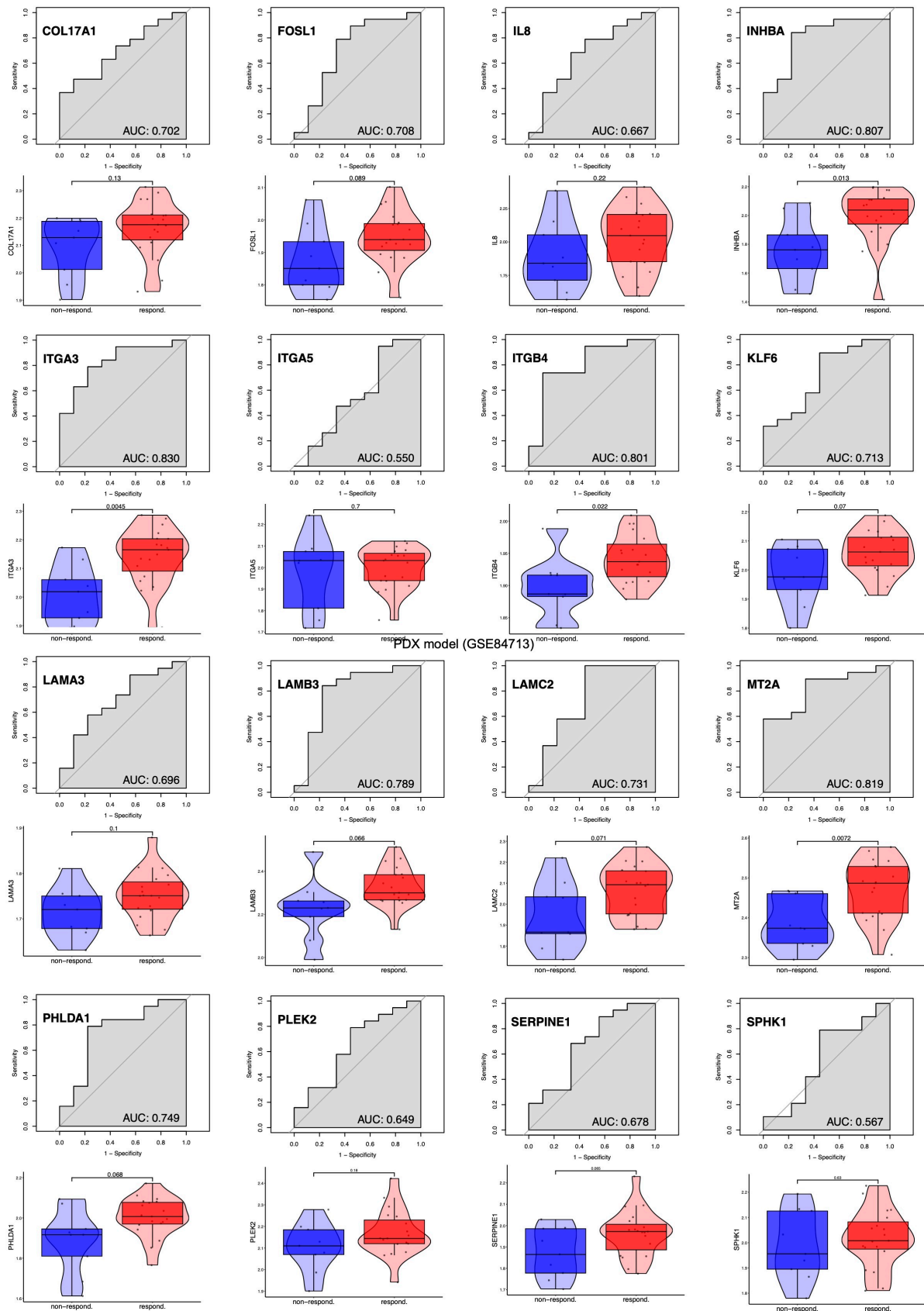




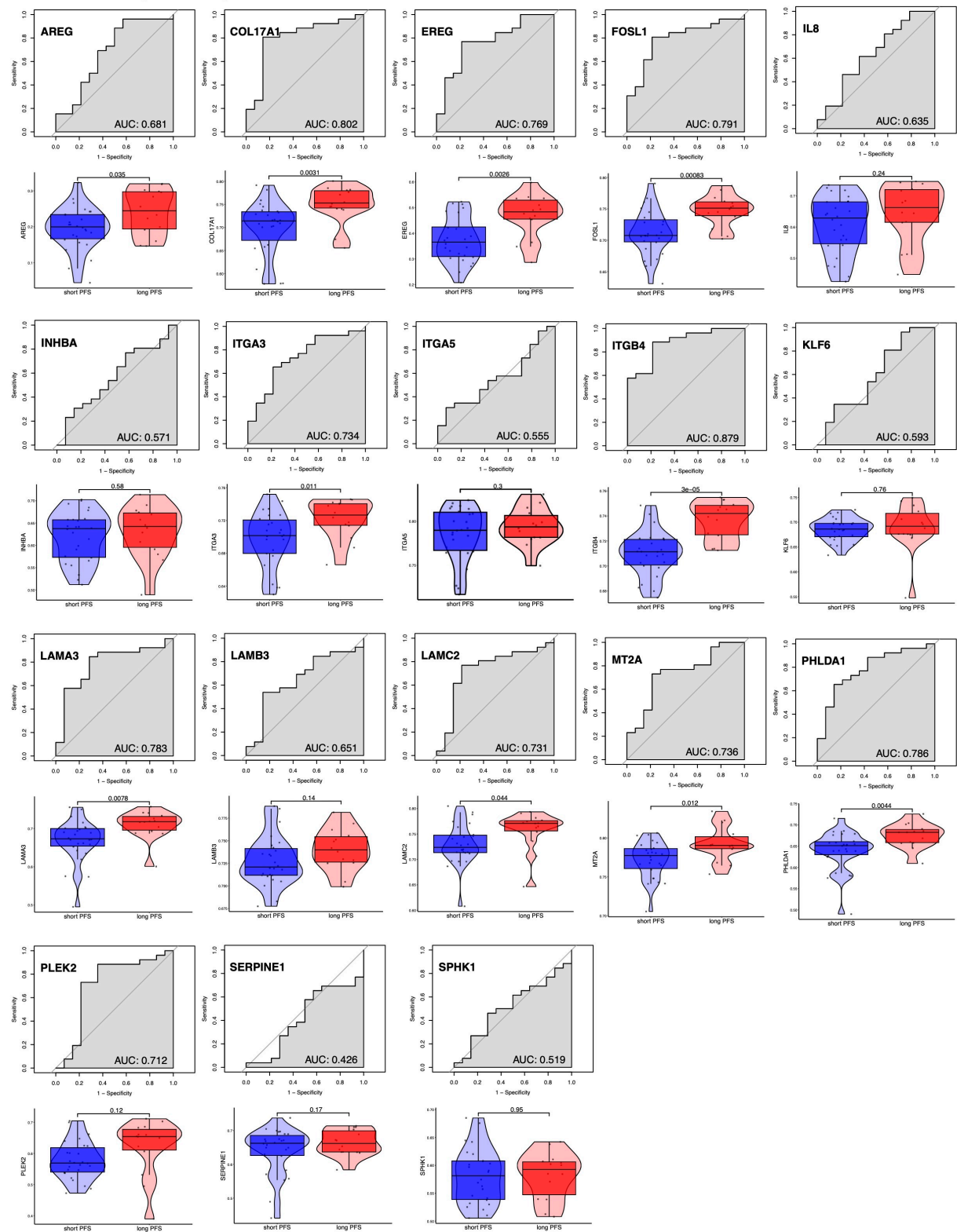
**Suppl. Figure 12: Interactions of HPV-neg. and -pos. malignant cells from GSE181919 with non-malignant cells**

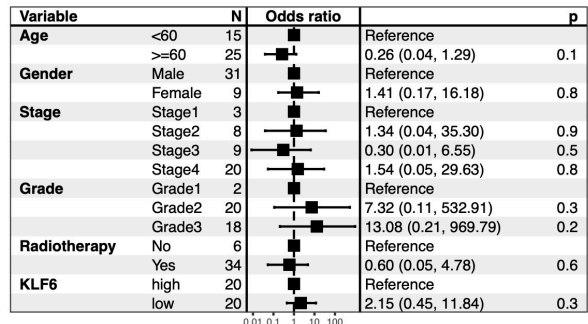
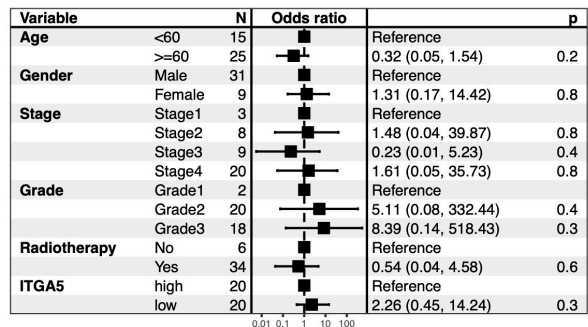
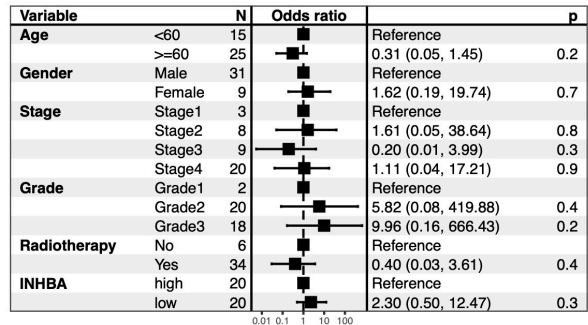
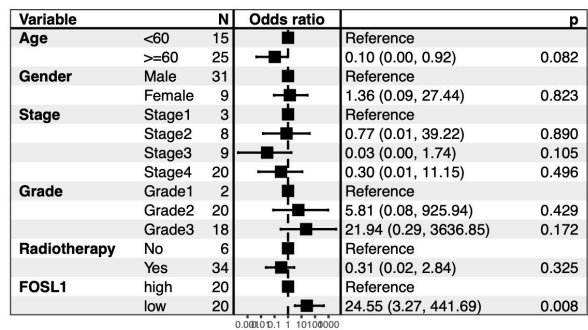
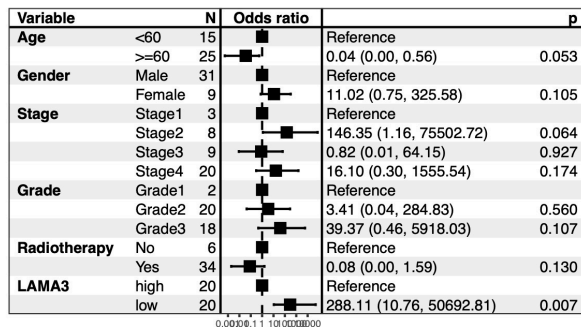
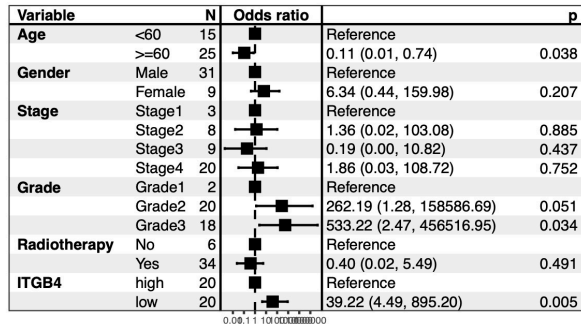
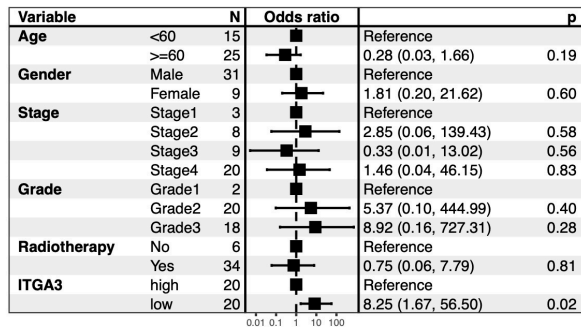
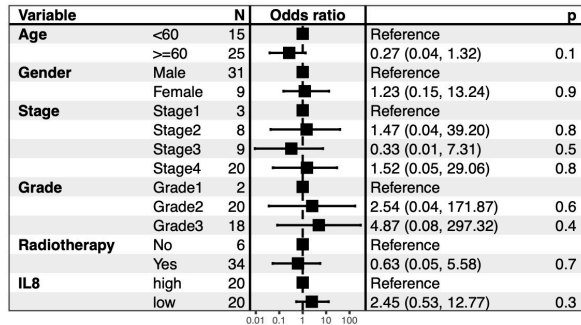
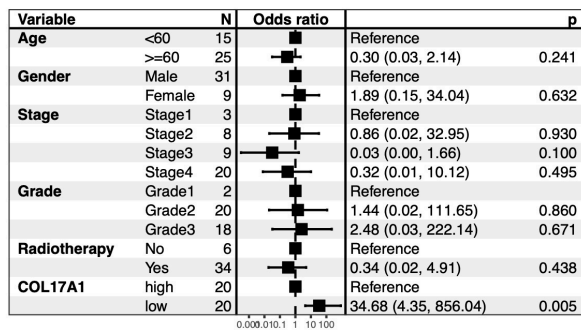
Interactions of malignant HPV-neg. (HPVn) and HPV-pos. (HPVp) cells from GSE181919 with B cells, CD4 and CD8 T cells, monocytes, dendritic cells, and fibroblast subtypes are shown together with numbers and interaction strength and ligand-receptor interaction (communication probability and p-value). **(A-D)** Interactions of cells of the “AREG” subtype with immune cells as indicated. **(E-H)** Interactions of cells of the “HBEGF” subtype with immune cells as indicated. **(I)** Interactions of cells of the “AREG” subtype with fibroblast subtypes. **(J)** Interactions of cells of the “HBEGF” subtype with fibroblast subtypes.

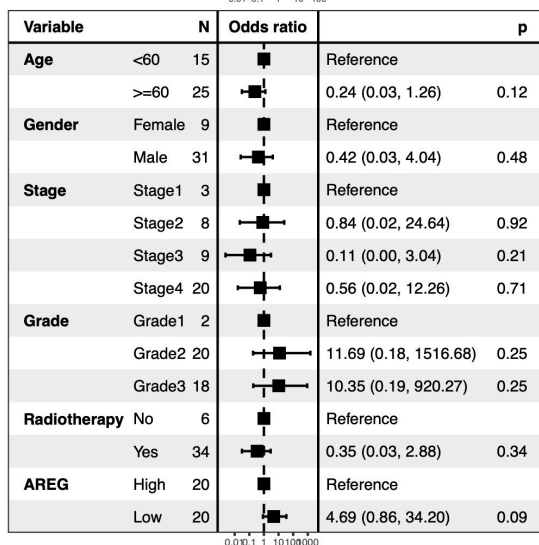
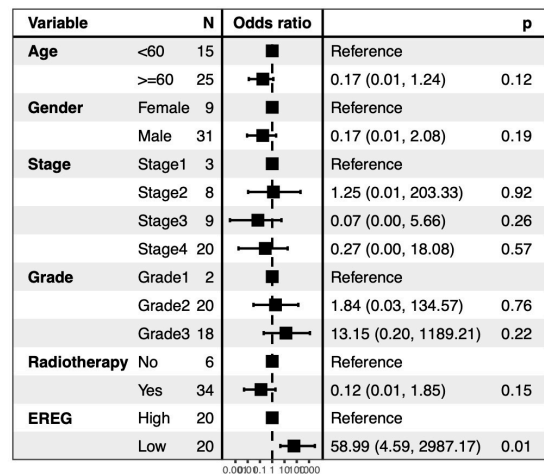
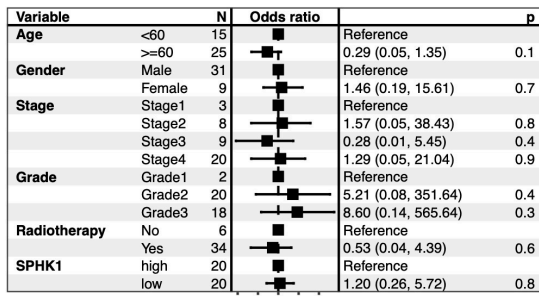
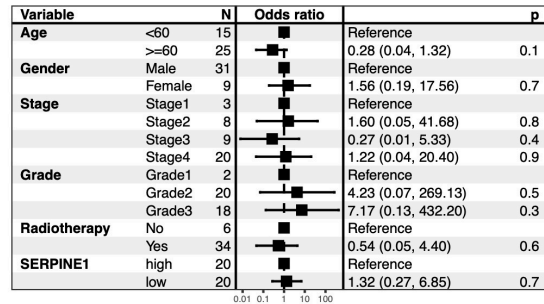
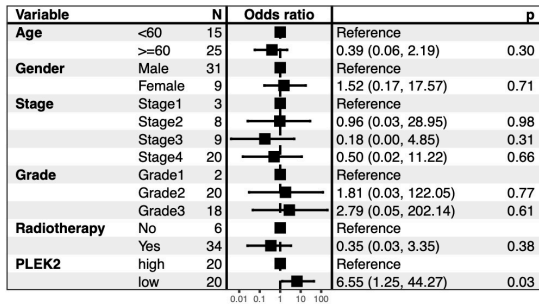
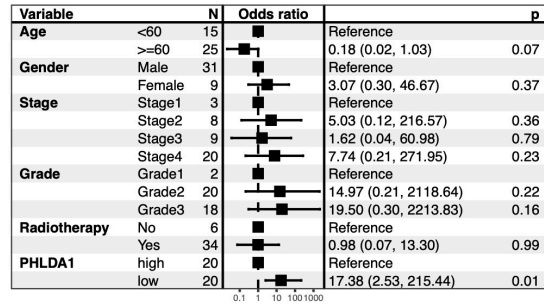
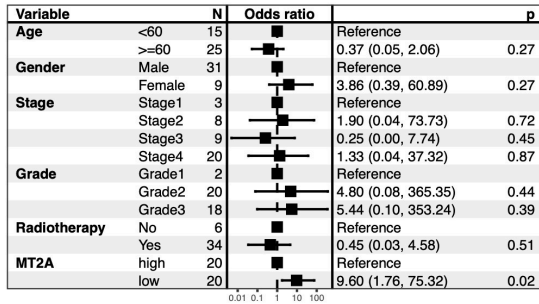
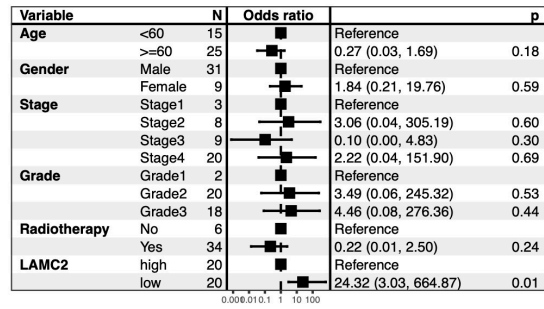
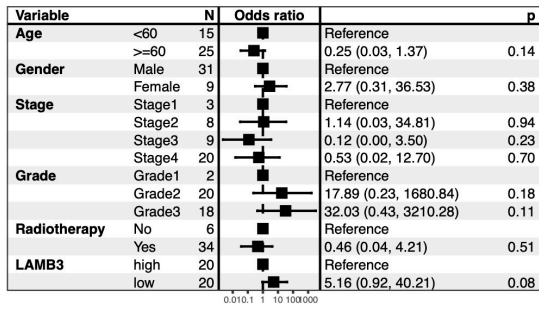


**PDX model (GSE84713)**

**Suppl. Figure 13: Correlation of fDEGs with Cetuximab response in a PDX-model of treatment**  
 Area under the curve (AUC) of receiver operating characteristic curves (ROC) for the association of the indicated genes with response to Cetuximab treatment in GSE84713 are shown in the upper graphs. Boxplot-whisker graphs are shown for the expression of the indicated gene with non-responder (blue) and responder (red) samples (displayed are: minimum, 1<sup>st</sup> quartile, median, 3<sup>rd</sup> quartile, maximum).

**A R/M-HNSCC (GSE65021)**

**B R/M-HNSCC Cetuximab treatment (odds of short PFS)**

**B R/M-HNSCC Cetuximab treatment (odds of short PFS)**



**Suppl. Figure 14: Correlation of fDEGs with Cetuximab response in R/M-HNSCC patients**

(A) Area under the curve (AUC) of receiver operating characteristic curves (ROC) for the association of the indicated genes with response to Cetuximab treatment in R/M-HNSCC patients (GSE65021) are shown in the upper graphs. Boxplot-whisker graphs are shown for the expression of the indicated gene with short progression-free survival (PFS; blue) and long-PFS (red) (displayed are: minimum, 1<sup>st</sup> quartile, median, 3<sup>rd</sup> quartile, maximum). (B) Multivariate linear regression model testing the odds to belong to the short progression-free survival (PFS) patient group. Shown are reference, p-values, odds with confidence interval for the parameters age, gender, stage, grade, radiotherapy, and fDEG (stratified at mean into high and low gene expression).